https://doi.org/10.5194/egusphere-2026-684
Preprint. Discussion started: 17 February 2026


# $CO_2$ and Heat exchange across the Nocturnal Canopy–Atmosphere interface in the Amazon rainforest

Anna C. Huitema[1], Vincent S. de Feiter[1], Raquel González-Armas[1], Oscar K. Hartogensis[1], Hella van Asperen[2], Cleo Quaresma Dias-Júnior[3], and Jordi Vilà-Guerau de Arellano[1]

[1]Meteorology and Air Quality section, Wageningen University, Wageningen, The Netherlands
[2]Biogeochemical Process Department, Max Planck Institute for Biogeochemistry, Jena, Germany
[3]National Institute for Amazonian Research, Manaus, Brazil

**Correspondence:** Anna C. Huitema (anna.huitema@wur.nl)

**Abstract.** We investigated the characteristics of the nocturnal boundary layer (NBL) above and within the Amazon rainforest canopy during the 2022 dry season. The study aims to determine how NBL dynamics influence nocturnal $CO_2$ and heat exchange across the canopy-atmosphere interface. Utilising observations from the CloudRoots-Amazon22 field campaign conducted at the Amazon Tall Tower Observatory, we distinguished between the strongly and weakly stable regimes to study the effect of radiative cooling and wind shear on $CO_2$ and heat exchange. Our results reveal a distinct, stable layer above the canopy with an average height of 150 to 188 m, which develops due to strong radiative cooling of the canopy top. Below the canopy, the cooling marks the build-up of a well-mixed layer within the canopy. In the weakly stable regime, increased turbulence at the canopy top was observed, leading to a significant observed $CO_2$ flux of 3.82 $\mu$mol m$^{-2}$ s$^{-1}$ above the canopy. In contrast, in the strongly stable regime, turbulence was almost absent, and the observed flux was only 0.16 $\mu$mol m$^{-2}$ s$^{-1}$, suggesting a decoupling of the canopy and the roughness sublayer. The decoupling was confirmed by the 2-3 times decreased vertical heat transport in the strongly stable regime. Even though our method includes typical observational uncertainties, our results show significant differences between $CO_2$ and heat exchange between the two regimes, stressing the importance of correctly representing the nocturnal dynamics in tall canopies like the Amazon Rainforest.

## 1 Introduction

The Amazon rainforest is considered a crucial terrestrial carbon sink in the global climate system (Science Panel for the Amazon., 2021; IPCC, 2023). However, as a result of climate change and deforestation practices (Costa and Foley, 2000), a decline in its uptake strength has been reported (Brienen et al., 2015; Hubau et al., 2020). Some studies suggest that the Amazon rainforest has already become a net carbon source (Aragão et al., 2014; Hubau et al., 2020; Gatti et al., 2021), while others continue to identify the Amazon as a net carbon sink (Harris et al., 2021). This disagreement largely stems from uncertainties in current modelling estimates, combined with the limited availability of high-quality observations to validate the models used (Rosan et al., 2024). Furthermore, especially during stratified nighttime conditions, the model representation of key processes in the soil-vegetation-atmosphere continuum remains inaccurate and incompletely evaluated (Cuxart et al., 2006; Hawkins and

https://doi.org/10.5194/egusphere-2026-684
Preprint. Discussion started: 17 February 2026


Sutton, 2009; Svensson et al., 2011; Anton Beljaars et al., 2011; van Stratum and Stevens, 2015; Vilà-Guerau de Arellano et al., 2023).

Stratified conditions form after sunset, when net longwave radiative cooling of the surface leads to the formation of a stable layer, referred to as the nocturnal boundary layer (NBL) (Mahrt et al., 1979; Garstang and Fitzjarrald, 1999). Accurately representing the $CO_2$ exchanges in the NBL remains challenging, particularly in tall canopies such as the Amazon rainforest (Bonan et al., 2018, 2021). Here, nocturnal radiative cooling cools the dense canopy top, forming a strong stable layer aloft (Mahrt, 1999). At the same time, nighttime autotrophic and heterotrophic respiration add $CO_2$ to the in-canopy atmosphere. Because of the strong atmospheric stability above the canopy top, the respired $CO_2$ is trapped within the canopy and accumulates over time (Mahrt, 1999). The extent to which the in-canopy atmosphere and stable layer aloft interact is governed by the intricate interplay of shear and buoyancy, which can either break, maintain or strengthen the present atmospheric stability (Stull, 1988; Mahrt, 1999). Interactions between these two layers predominantly occur at the canopy-atmosphere interface, affected by the characteristics and processes of both the in-canopy and the roughness sublayer aloft (De Kauwe et al., 2017).

To describe the canopy-atmosphere interactions in the NBL, studies often subdivide the available observations into two regimes: a strongly stable and a weakly stable regime (Mahrt, 1998; Oliveira et al., 2013, 2018). In the strongly stable regime, radiative cooling dominates, leading to an almost complete absence of turbulence. In the weakly stable regime, shear-driven turbulence is dominant, resulting in weak turbulent motions that limit the stratification. In addition to the two regimes, often a third regime is added, the intermittent regime, characterised by bursts of intermittent turbulence, defined as brief periods of increased turbulent activity, typically observed during strongly stable conditions (Acevedo et al., 2008; Van de Wiel et al., 2002a, b). The generated turbulence, during intermittent and weakly stable periods, allows interactions between the canopy and stable layer, redistributing $CO_2$ from the canopy layer to the air aloft (Smedman, 1988; Mahrt, 1998; Karipot et al., 2006; Acevedo et al., 2008; Oliveira et al., 2013). Because weakly and strongly stable regimes differ markedly in atmospheric turbulence, they lead to different interaction dynamics at the canopy–atmosphere interface (Oliveira et al., 2018). Therefore, to understand the $CO_2$ exchange between the canopy layer and atmosphere aloft, a more detailed characterisation of the NBL structure and exchange dynamics is essential.

To this end we will use the comprehensive in-canopy and above-canopy observations from the CloudRoots-Amazon22 (hereafter referred to as CloudRoots) field campaign (Vilà-Guerau de Arellano et al., 2024) to perform an in-depth characterisation of the NBL, aiming to enhance our understanding of the processes that drive $CO_2$ exchange between the canopy and atmosphere aloft. We distinguish between the strongly and weakly stable regimes to clearly differentiate the $CO_2$ and heat exchange between the two turbulent regimes (Section 2.2). We study the interactions between the stable atmosphere above the canopy and within-canopy air, using the governing equations of TKE, heat and $CO_2$ (Section 2.5). The governing equations describe the changes in atmospheric properties over time (Stull, 1988). By analysing these three equations, we gain insight into how the NBL is influenced by the production of shear and radiative cooling and how this affects the exchange of $CO_2$ and heat in the atmosphere, specifically between the canopy and atmosphere aloft. However, before we begin quantifying $CO_2$ and heat exchange utilising the governing equations, it is important to understand the temporal evolution of both the above and within-canopy atmosphere and their degree of coupling. For a first indication of the stability regime above the canopy during

https://doi.org/10.5194/egusphere-2026-684
Preprint. Discussion started: 17 February 2026


the CloudRoots campaign, we calculate the boundary layer height ($h_{NBL}$) using five different criteria of potential temperature ($\theta$), $CO_2$, horizontal wind speed ($U$), the Richardson number (Ri) and turbulent kinetic energy (TKE) (Section 2.3). The $h_{NBL}$ is an important indicator for the turbulent state and associated exchange of $CO_2$ (Culf et al., 1997). Besides the stability of the above canopy atmosphere, we connect our explanation to the dynamic behaviour of the nocturnal canopy, because a significant flux of $CO_2$ originates from within the canopy (Moonen et al., 2025). Therefore, we quantify the stability of the canopy layer, using vertical profiles of $\theta$ and $CO_2$ (Section 2.4), gaining insight into the degree of decoupling between the canopy and stable layer above. This section is completed by discussing and quantifying the degree of coupling between the in and above canopy using the Richardson gradient number that integrates the turbulent shear and the stratifying effects by longwave radiative divergence.

## 2 Methods

### 2.1 CloudRoots-Amazon22 campaign

Observations were collected at the site of the Amazon Tall Tower Observatory (ATTO) (-2.15° N, -59.01° E) and in its immediate surroundings. The measurement period was during the dry season from 8 to 21 August 2022. The campaign aimed to improve the understanding of interactions between the cloud-vegetation-surface system. The range of observations made allowed us to study interactions across multiple scales, from the leaf level to the atmospheric boundary layer.

The characteristics of the area surrounding ATTO are described in more detail by Andreae et al. (2015). We summarise the most relevant information for this study. The location of ATTO is approximately 150 km Northeast of Manaus. At the ATTO site, three measuring towers are present of which we will be using two: the 325 m ATTO tall tower and the shorter 81 m Instant tower. The towers are located on top of a plateau (ca. 120 m above mean sea level) in the central Amazon. The plateau is characterised by small-scale topography, with maximum elevation changes of 100 m. The average tree height is 20.7 $\pm$ 0.4 m, but the tallest trees reach 36-40 m. For the study, we defined the aerodynamic canopy top as 32 m following González-Armas et al. (2025). Sensors were placed at 15 height levels between the two towers, continuously monitoring atmospheric variables, trace gases, and turbulent fluxes. The nocturnal period is defined in this study as the period between sunset (18:00 LT) and sunrise (06:00 LT), where LT, local time, is UTC-4 hr.

We used 30-minute averaged turbulent fluxes, and vertical profiles of windspeed and temperature constructed from measurements at the following heights: 5, 15, 25, 35, 50, 81 m on the Instant tower, and 100, 127, 151, 172, 196, 223, 247, and 298 m on the ATTO tall 90 tower. Moisture and CO2 fluxes were measured at 5, 25, 50, 81 and 196 m. The CO2 molar fraction was averaged over 15-minute intervals and measured on the Instant tower with a Picarro Gas Analyser at 4, 24, 38, 53 and 79 m and one additional level at the ATTO tall tower, at 321 m. From the tower measurements, we construct connected vertical profiles between the surface and 300 m by combining measurements from both the Instant and ATTO tall tower (Mendonça et al., 2025a). All instrument and sampling details specific to the CloudRoots campaign can be found in Vilà-Guerau de Arellano et al. (2024) and for the permanent instrumentation in Mendonça et al. (2025a).

https://doi.org/10.5194/egusphere-2026-684
Preprint. Discussion started: 17 February 2026


**Table 1.** Six criteria used to distinguish between strongly and weakly stable regimes for the CloudRoots campaign. The subscripts for U, Ri, TKE, and $u_*$ indicate that the threshold was determined for observations at 50 m. The $Ri_c$ is taken as 0.25.

| Vertical Profile | Strongly Stable | Weakly Stable | Reference |
|---|---|---|---|
| $\theta$ | $\Delta\theta_{50-25} > 1.5$ K | $\Delta\theta_{50-25} < 1.5$ K | (Stull, 1988; Culf et al., 1997) |
| $CO_2$ | $\Delta CO_{2,79-38} > 10$ ppm | $\Delta CO_{2,79-38} < 10$ ppm | (Stull, 1988; Culf et al., 1997) |
| $U$ | $U_{50} < 2.5$ m s$^{-1}$ | $U_{50} > 2.5$ m s$^{-1}$ | (Sun et al., 2012; Dias-Júnior et al., 2017) |
| $Ri$ | $Ri_{50} > Ri_c$ | $Ri_{50} < Ri_c$ | (Grachev et al., 2013) |
| $TKE$ | $TKE_{50} < 0.1$ m$^2$ s$^{-2}$ | $TKE_{50} > 0.1$ m$^2$ s$^{-2}$ | (Banta et al., 2003; Sun et al., 2012) |
| $u_*$ | $u_{*,50} < 0.1$ m s$^{-1}$ | $u_{*,50} > 0.1$ m s$^{-1}$ | (Loescher et al., 2006; Aubinet, 2008) |

### 2.2 Criteria for assessing strongly and weakly stable regimes

To distinguish between the strongly and weakly stable regimes, we employed six criteria ($\theta$, $CO_2$, $U$, $Ri$, $TKE$, $u_*$) from previous characterisation studies, adjusted to the CloudRoots observations (Table 1). In order to classify a profile within a regime, all six criteria must be met. Since the difference between the regimes is most pronounced in the layer above the canopy due to strong stratification, we formulated the criteria thresholds within this layer. The first two criteria are based on atmospheric gradients, which form as a result of radiative cooling at the canopy top. More specifically, the criteria are based on gradients between 50 and 25 m for $\theta$ and 79 and 39 m for $CO_2$. We determined thresholds on the degree of stratification (Stull, 1988) (Table 1), which are consistent with the strongly and weakly stable characterisation reported by Culf et al. (1999).

### 2.3 Criteria for assessing the nocturnal boundary layer height

To estimate $h_{NBL}$, we compared five criteria on the vertical profiles of $\theta$, $CO_2$, $U$, $Ri$ and $TKE$ above the canopy top. The five variables on which the criteria are applied are illustrated in Fig. 1, highlighting the differences between the strongly (red) and weakly (blue) stable stratified regimes. To not limit ourselves to $h_{NBL}$ at measuring heights, we fitted a 2nd-order logarithmic function to vertical profiles of $\theta$, $CO_2$ and $U$ (Stull, 1988). For $Ri$ and $TKE$, vertical profiles are linearly interpolated to reflect the observed non-logarithmic pattern in $Ri$ and $TKE$. For future reference, we indicate the calculated $h_{NBL}$ as $h_{criteria}$ for each of the criteria. In the following, we elaborate on each of the five criteria in more detail. We applied the criteria to the data spanning 8 to 19 August; we excluded the last two days of the field campaign because of data limitations.

In the NBL, $\theta$ increases with height. However, this increase is not uniform; near the canopy, the vertical gradient is large, while toward the top of the NBL, the gradient weakens and gradually approaches zero. Therefore, we defined the NBL height as the lowest height at which the vertical gradient of $\theta$ falls below a prescribed low threshold (Fig. 1a). This threshold was defined as 0.003 m$^{-1}$. To reach the threshold. $\theta$ values were normalised as $\theta_N = \theta/\Delta\theta$, where $\Delta\theta$, is the difference between the potential temperature at 300 m (top tower) and 32 m (canopy top). The normalisation eliminates temperature differences

https://doi.org/10.5194/egusphere-2026-684
Preprint. Discussion started: 17 February 2026


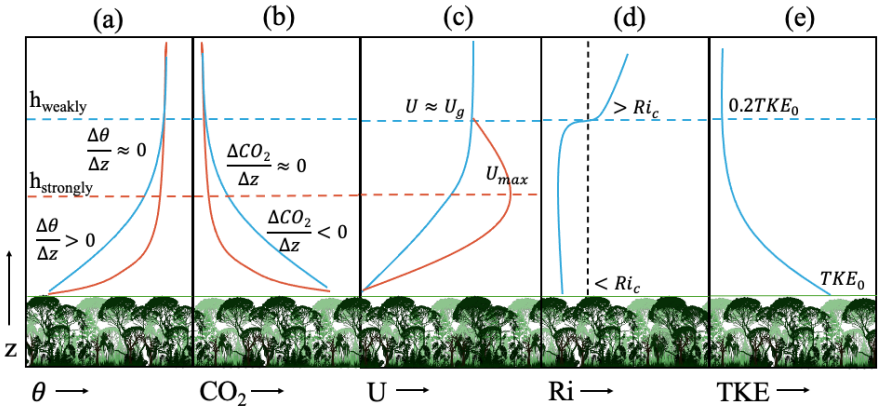


**Figure 1.** Five criteria of estimating the nocturnal boundary layer height ($h_{NBL}$): (a) potential temperature ($\theta$), (b) $CO_2$, (c) wind speed ($U$), (d) Richardson number ($Ri$) and (e) turbulent kinetic energy ($TKE$). The blue lines represent the weakly stable regime and the red lines the strongly stable regime. The blue and red horizontal dashed lines indicate the estimated $h_{NBL}$ of the weakly and strongly stable profiles, respectively. The vertical dashed black line in (d) represents the critical Richardson number (0.25).

between nights and the beginning and end of a single night, resulting in vertical profiles that are easy to compare. Nevertheless, it does not have a significant effect on the calculated $h_\theta$.

Contrary to $\theta$, for $CO_2$, the NBL is characterised by a negative $CO_2$ gradient with height, approaching 0 ppm $m^{-1}$ near the top of the stable layer. Similar to $\theta$, we normalised the $CO_2$ gradient with height and relaxed the threshold. This threshold is defined as 0.0025 $m^{-1}$ (Fig. 1b).

The $U$ criterion was subdivided into two parts, based on whether a nocturnal low-level jet (NLLJ) Blackadar (1957) is observed above the NBL or not. When an NLLJ is present above the NBL, we found $h_U$ at the height where $U = U_{max}$ (red line Fig. 1c), as the NLLJ wind maximum forms on top of the stable NBL, where atmospheric friction approaches zero (Mendonça et al., 2025b). When no NLLJ is present, we found $h_U$ where $U = U_g$ (blue line Fig. 1c), with $U_g$ being the geostrophic wind. We assume that the windspeed reaches $U_g$ at the highest measuring level (298 m), due to decreased friction present in the residual layer above the NBL. To obtain realistic estimates, we relaxed the threshold to $U = U_g \pm 0.3$ m $s^{-1}$.

The final two methods, based on $Ri$ (calculated as the gradient Richardson number) and $TKE$, are only applied in the weakly stable regime, as sufficient turbulence above the canopy is required for the application of the criteria. The methods are based on the assumption that all turbulence has dissipated in the residual layer, where the atmosphere is neutral. Therefore, $h_{Ri}$ is found when $Ri \geq Ri_c$ for weakly stable profiles (Fig. 1d) and $h_{TKE}$ is determined where $TKE$ has been largely reduced compared to its value at the canopy top, we assumed $TKE = 0.2TKE_0$ due to predominantly stable conditions during the observations period (Fig. 1e). Here, $TKE_0$ is the observed $TKE$ value at the canopy top.

https://doi.org/10.5194/egusphere-2026-684
Preprint. Discussion started: 17 February 2026


### 2.4 Temporal evolution of stability within and above the canopy

Following the classification of the regimes and $h_{NBL}$, we studied the temporal evolution of atmospheric stability, focusing on both the in-canopy atmosphere, the stable layer aloft and the interaction at the canopy-atmosphere interface. Furthermore, to compare the stability of the in-canopy and stable layer aloft, we introduce $Ri$ for the stable layer and canopy atmosphere based on the work of Oliveira et al. (2013). For the stable layer above canopy, the Richardson number ($Ri_{atm}$) is defined by Eq. 1, and for the in-canopy layer, the Richardson number ($Ri_{can}$) is determined by Eq. 2. In the equations, the subscripts of $\theta$ and $U$, indicate the measurement heights of $\theta$ and $U$, $\Delta z$ is the difference in height between the two heights indicated in the subscripts, $\theta_{ref}$ is a reference temperature, taken as the potential temperature at the highest measuring level on ATTO (298 m). To explicitly study the difference between the strongly and weakly stable regimes, we selected a predominantly strongly stable night and a predominantly weakly stable night.

$$Ri_{atm} = \frac{g\Delta z}{\theta_{ref}} \frac{\theta_{81} - \theta_{35}}{(U_{81} - U_{35})^2} \tag{1}$$

$$Ri_{can} = \frac{g\Delta z}{\theta_{ref}} \frac{\theta_{35} - \theta_{5}}{(U_{35} - U_{5})^2} \tag{2}$$

### 2.5 Quantifying canopy-atmopshere exchange of $CO_2$ and heat

To assess and quantify the coupling and exchange between the in-canopy atmosphere and the stable layer aloft, we evaluated the governing equations of TKE, heat and $CO_2$ for the observed strongly and weakly stable regimes that satisfy all six criteria as listed in Table 1 and discussed in Section 2.2. This ensures that we explicitly study the difference between the two regimes and not other processes. To evaluate the governing equation with our observations, we made the following two assumptions: 1) The atmosphere is horizontally homogeneous ($\frac{\partial \psi}{\partial x} = \frac{\partial \psi}{\partial y} = 0$) and 2) subsidence is negligible ($\overline{w} = 0$) are done. In addition, we aligned the coordinate system with the mean wind such that only the $u$ component of the wind remained. We evaluated the governing equations using 30-minute averaged data (indicated by the overbars). Vertical derivatives were calculated using one level above and below the desired height, except for the vertical divergence of the $CO_2$ flux, for which, due to a lack of measurements at all levels, a first-order method was employed, which may affect the accuracy of the calculations. The residual ($R$) or non-closure of the budgets resulted from calculation uncertainty due to contributions from neglected terms that could not be calculated with our observations, and the observation uncertainty. In the following, we explain each equation individually.

#### 2.5.1 Governing equation of TKE

Using the available observations, we analysed the $TKE$ budget. Due to observational limitations, we simplified the TKE governing equation to five terms (Eq. 3). The net tendency of $TKE$ ($\frac{\partial \overline{e}}{\partial t}$), which is controlled by four terms, which from left to right are: the buoyant consumption (term 1), shear production (term 2), dissipation of $TKE$ (term 3) and the residual term ($R_{TKE}$) (term 4). The $R_{TKE}$ term contains processes that could not be quantified with current observations: the pressure fluctuation

https://doi.org/10.5194/egusphere-2026-684
Preprint. Discussion started: 17 February 2026


gradient term, the turbulent transport term and the advection of $TKE$ term. In Eq. 3 $g$ is the gravitational acceleration (9.81 m s$^{-2}$), $\theta_v$ the virtual potential temperature in K, $\overline{w'\theta'_v}$ the kinematic heat flux in K m s$^{-1}$ and $\overline{u'w'}$ the momentum flux in m$^2$ s$^{-2}$. The dissipation ($\epsilon$) is parameterised as $\epsilon = 15\upsilon(u^2/\lambda^2)$, where $\lambda$ is the buoyancy length scale, calculated according to $\lambda = \sigma_w/N_{BV}$ (Stull, 1988). Here $\sigma_w$ is the variance of the vertical wind and $N_{BV}$ is the Brunt–Väisälä frequency, known as the frequency at which air parcels oscillate in stable conditions, defined as $N^2_{BV} = g/\overline{\theta_v}\,\partial\theta_v/\partial z$ (Stull, 1988).

$$\frac{\partial \overline{e}}{\partial t} = \frac{g}{\overline{\theta_v}}\overline{w'\theta'_v} - \overline{u'w'}\frac{\partial \overline{u}}{\partial z} - \epsilon + R_{TKE} \tag{3}$$

### 2.5.2 Governing equation of heat

Using the available observations we analysed the governing equation of heat (Eq.4). In Eq. 4 the net tendency of $\theta$ ($\partial\overline{\theta}/\partial t$), is controlled by three terms, from left to right: the turbulent transport of heat (term 1), the radiative cooling (term 2), positive towards the surface) and $R_\theta$ (term 3). Here, $\rho$ is the air density in kg m$^{-3}$, $c_p$ the specific heat of air at constant pressure (1004 J K$^{-1}$ kg$^{-1}$) and $Q$ the net longwave radiation in W m$^{-2}$. The $R_\theta$ encompasses the molecular diffusion term, the latent heat term and the advection of heat (Stull, 1988). We expected the latent heat release to approach zero at night (de Abreu Sá et al., 1988). The latter could be confirmed by the absence of fog or dew observations during the nights studied.

Longwave radiation observations during CloudRoots were scarce; only one sensor (at 75 m) measured incoming and outgoing radiation. As a result, the long wave radiation cooling term ($1/\rho cp\; dQ/dz$) could not be determined from our observations. We therefore estimated radiative cooling using the Radiative Transfer for Energetics + RRTM for General Circulation Model – Parallel (RTE+RRTMGP) (Pincus et al., 2019). Specifically, we used the open-source C++ interface to RTE+RRTMGP (van Heerwaarden et al., 2025). To run the model, we estimated radiation profiles based on the temperature and moisture vertical profiles of ECMWF Reanalysis 5th Generation data (ERA5) (Hersbach et al., 2020). The ERA5 profiles were downscaled with the "Large-eddy simulation and Single-column model—Large-Scale Dynamics" or (LS)$^2$D in short (van Stratum et al., 2023). Finally, we ran the model utilising default clear sky settings and disabled shortwave radiation. To test the reliability of the model output, we compared tower observations with ERA5 vertical profiles (Appendix A). The profiles agree with each other with a maximum difference of 2 K in the temperature profiles and 0.004 ppmv for the volume mixing ratio (vmr), which is sufficient to get a realistic estimate of radiative cooling. This assumption was confirmed when we compared the model output at 75 m to the tower observations (Appendix A), which show absolute differences between 1 - 12 W m$^{-2}$, depending on the selected moment.

$$\frac{\partial \overline{\theta}}{\partial t} = -\frac{\partial \overline{w'\theta'}}{\partial z} + \frac{1}{\overline{\rho} c_p}\frac{\partial \overline{Q}}{\partial z} + R_\theta \tag{4}$$

### 2.5.3 Governing equation of $CO_2$

Finally, we analysed the governing equation of $CO_2$ (Eq. 5), using our observations. In the equation, three terms remain after the made assumptions, the net $CO_2$ tendency ($\partial\overline{CO_2}/\partial t$), controlled by from left to right: the turbulent transport of $CO_2$ (term

https://doi.org/10.5194/egusphere-2026-684
Preprint. Discussion started: 17 February 2026


**Table 2.** Selected times for the weakly and strongly stable regimes, with the abbreviations used further in the study.

| Time (LT) | Regime | Abbreviation |
|---|---|---|
| 11 August 2022 02:00 | Strongly stable | S1 |
| 11 August 2022 03:00 | Strongly stable | S2 |
| 13 August 2022 02:00 | Strongly stable | S3 |
| 13 August 2022 03:00 | Strongly stable | S4 |
| 13 August 2022 22:00 | Weakly stable | W1 |
| 13 August 2022 23:00 | Weakly stable | W2 |
| 18 August 2022 21:00 | Weakly stable | W3 |
| 18 August 2022 22:00 | Weakly stable | W4 |

1) and the residual term $R_{CO_2}$ (term 2). Here $\overline{w'CO_2'}$ is the $CO_2$ flux in ppm m $s^{-1}$. The molecular viscosity was neglected, similar to the conservation equation of heat. The $R_{CO_2}$ encompasses the molecular diffusion term, potential sources and sinks of $CO_2$ and advection of $CO_2$.

$$\frac{\partial \overline{CO_2}}{\partial t} = -\frac{\partial \overline{w'CO_2'}}{\partial z} + R_{CO_2} \tag{5}$$

## 3 Results

The results are subdivided into three sections. The first two sections describe the temporal evolution of the NBL during the complete CloudRoots campaign (8-19 August). Section 3.1 describes the evolution of the $h_{NBL}$ over time, comparing the five criteria (Section 2.2). Section 3.2 describes the temporal evolution, hereby distinguishing between the within and above canopy layers. Finally, in Section 3.3, we evaluate the governing equations utilising the nights classified as strongly and weakly stable, based on the six criteria (Table 1). We found only eight hours in which all strongly/weakly stable criteria are valid. The designated hours are spread across four nights, with each night represented by two consecutive hours (Table 2).

### 3.1 Nocturnal boundary layer height

The estimates of $h_{NBL}$ for the five criteria ($\theta$, $CO_2$, U, Ri, TKE) are presented together with the overall mean $h_{avg}$ (grey line) in Fig. 5. In Fig. 5b-f, we present the hourly variation between the 11 nights in $h_{NBL}$ for each criterion separately. We found values of $h_{NBL}$ ranging from 114 to 241 m amongst all criteria, where $h_{Ri}$ gives the lowest- and $h_{TKE}$ gives the highest estimate. The 11 night average, $h_{NBL}$ was between 150 and 188 m (Fig. 5a - grey line).

The estimation of $h_\theta$ (Fig. 5b) most closely follows the mean, with an average value of 165 $\pm$ 28.4 m. In addition, compared to the other four criteria, the median of $h_\theta$ is closest to $h_{avg}$. The $h_{CO_2}$ is estimated to be 156 $\pm$ 42.6 m (Fig. 5c) which is

https://doi.org/10.5194/egusphere-2026-684
Preprint. Discussion started: 17 February 2026


lower compared to $h_{avg}$. Interestingly, the median of $h_{CO_2}$ remained around 140 m throughout the night, indicating that the variation is caused by a few high $h_{CO_2}$ values. We hypothesise that these higher values could be caused by potentially bursts of intermittent turbulence (Karipot et al., 2006; Oliveira et al., 2013). For both $h_\theta$ and $h_{CO_2}$, the variation increases between 00:00-01:00 LT and 05:00-06:00 LT, indicating enhanced turbulence. Increased turbulence around this time was also observed in the study of Oliveira et al. (2018).

Estimations of $h_U$ (Fig. 5d) are found to be 195 $\pm$ 63.4 m. The large variation in $h_U$ is attributed to nights with almost linear vertical wind profiles (high $h_U$, see Fig. 1) and nights with an NLLJ (low $h_U$, see Fig. 1). Linear wind profiles were present on the nights between 13 and 17 August. Weak NLLJ, with maximum wind speeds above $h_{NBL}$ of 5.5 m s$^{-1}$, were observed during the nights of 12-13 August and 17-18 August.

For $h_{Ri}$ and $h_{TKE}$, it is important to stress that these values were only calculated during periods with sufficient turbulence (weakly stable periods). The limited number of calculations, particularly influences results for $h_{TKE}$, as it could only be calculated in 20% of the analysed hours. The calculation of $h_{Ri}$ had an average of 134 $\pm$ 28.6 m (Fig. 5e), being below $h_{avg}$. Additionally, it is observed that $h_{Ri}$ is often significantly lower than $h_\theta$ and $h_{CO_2}$, during turbulent periods. The $h_{TKE}$ is calculated to be 195 $\pm$ 60.0 m (Fig. 5f), which is higher than the $h_{avg}$, and it exhibits significant variation, partly due to the limited number of estimations.

When we take into account both the average and variation of $h_{NBL}$ utilising all five criteria, $h_\theta$ can be seen as the most reliable estimate of $h_{NBL}$. However, given the large daily and hourly variations observed for all five criteria, we used $h_{avg}$ as our estimate for $h_{NBL}$ in this study.

To put our results into perspective, we compared them to previous studies. The $h_{NBL}$ above the Amazon rainforest has been investigated in a limited number of studies. All these studies reported $h_{NBL}$ values ranging from 80 m to 250 m (Oliveira et al., 2018; Carneiro and Fisch, 2020; Mendonça et al., 2025a), which is in line with our results. We analysed the study by Mendonça et al. (2025a) in a bit more detail, as it investigated $h_{NBL}$ at ATTO using one year of data (2022), including the CloudRoots observation period. Mendonça et al. (2025a) found $h_{NBL}$ to vary between 81 and 223 m, similar to the range depicted in Fig. 5a. With this finding, we showed that, contrary to the expectations of Mendonça et al. (2025a), indirect turbulent measurements yield trustworthy results for $h_{NBL}$, as our calculated $h_{NBL}$ closely aligns with their estimate of $h_{NBL}$, and does not show large fluctuations. In addition, we found that NLLJ formation (associated with low turbulence) occurred under Northeast winds, in line with the lower roughness area to the Northeast and associated lower $h_{NBL}$ in Mendonça et al. (2025a).

Finally, to connect our results to the two regimes, we calculated the average $h_{NBL}$ for the four strongly stable and the four weakly stable periods. For the strongly stable regime, we found an average $h_{NBL}$ of 130.0 m, and for the weakly stable regime, we found an average $h_{NBL}$ of 180.3 m. In the weakly stable periods, the $h_{NBL}$ is significantly higher than during strongly stable periods, highlighting the capability of the relatively simple $h_{NBL}$ estimations for a first indication of the turbulent state of the atmosphere.

https://doi.org/10.5194/egusphere-2026-684
Preprint. Discussion started: 17 February 2026


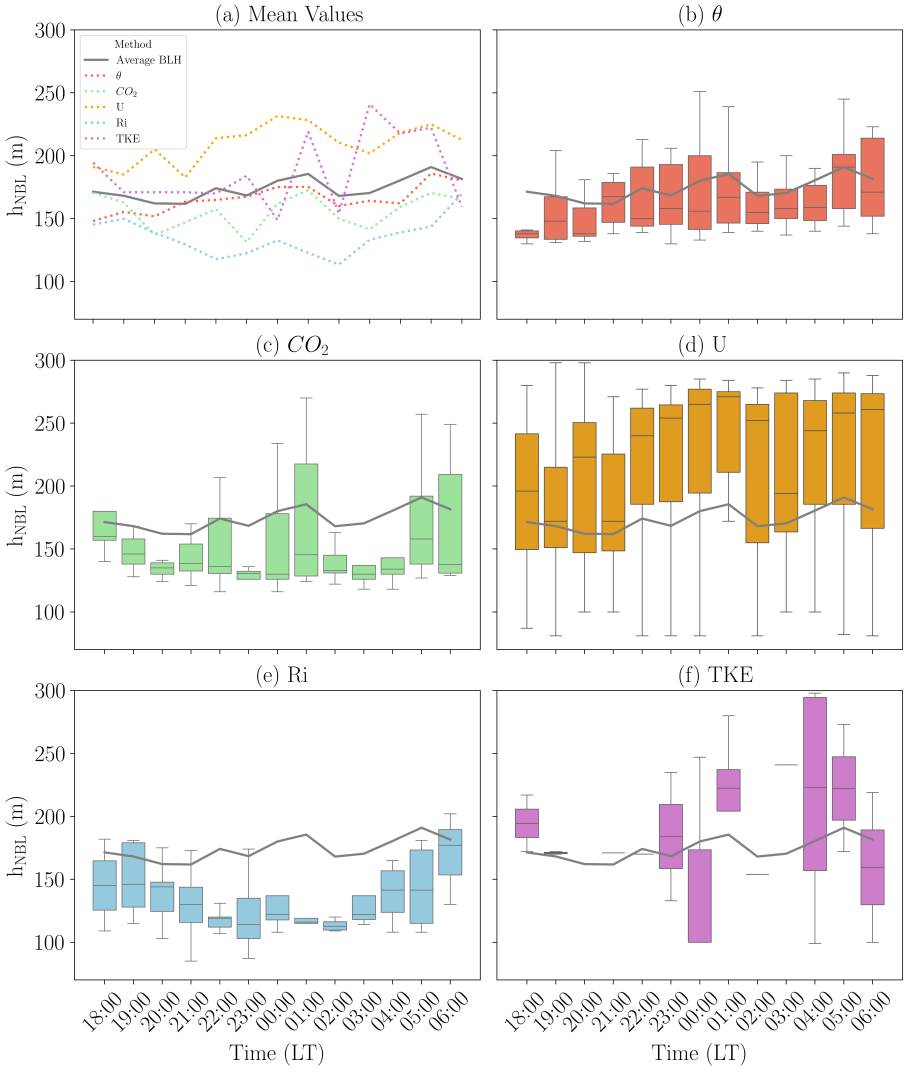


**Figure 2.** Hourly nocturnal boundary layer height in LT (UTC-4), estimated for the period between 8 and 19 August 2022. Panel (a) gives the mean boundary layer height for each of the five criteria ($\theta$, $CO_2$, U, $Ri$ & $TKE$) and the average of those five criteria (grey line). The remaining five graphs give the variation between the nights for every hour, for (b) potential temperature ($\theta$), (c) $CO_2$, (d) windspeed ($U$), (e) Richardson number ($Ri$) and (f) turbulent kinetic energy ($TKE$). Here, the grey line represents the five-criterion mean boundary layer height.

### 3.2 Temporal evolution of stability within and above the canopy

In Fig. 3, average vertical profiles for $\theta$ and $CO_2$ are presented for two-hour averaged periods. Above 25 m the stability of the atmosphere increases over time, we observed an increase (decrease) in the $\theta$ ($CO_2$) gradient from 0.040 K m$^{-1}$ (-0.09 ppm m$^{-1}$) at sunset to 0.046 Km$^{-1}$ (-0.51 ppm m$^{-1}$) at sunrise between 25 (24) and 81 (79) m. In contrast, below 25 m, the

https://doi.org/10.5194/egusphere-2026-684
Preprint. Discussion started: 17 February 2026


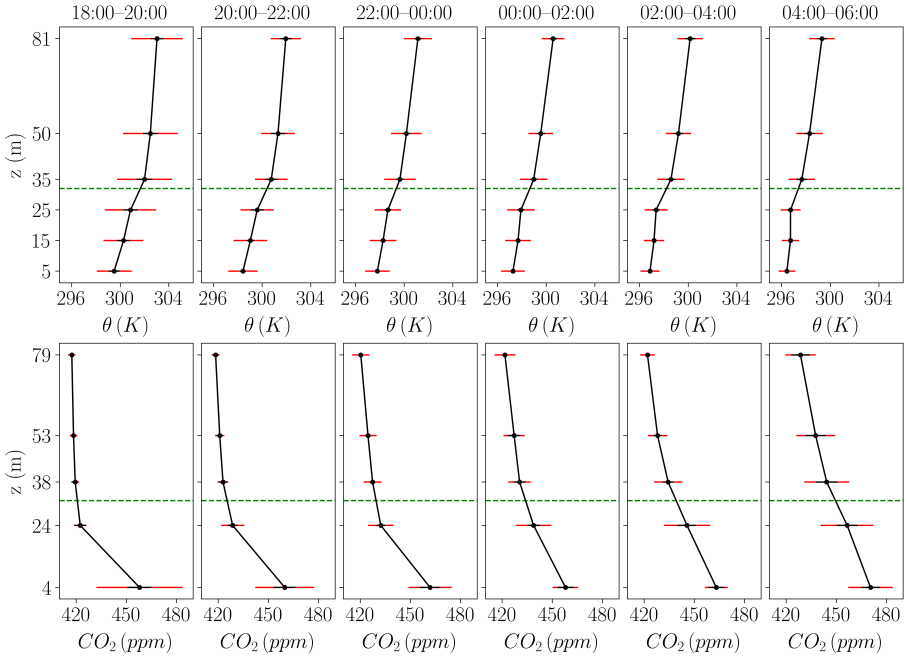


**Figure 3.** Mean profiles of potential temperature (top) and $CO_2$ (bottom) during the night after shallow convective days, averaged for every 2 hours. Red error bars are the standard deviation between the different nights, and the black error bars indicate the average 2-hour bin variation. The striped green horizontal line indicates the aerodynamic canopy top at 32 m.

$\theta$ ($CO_2$) gradient decreased (increased) from 0.067 K $m^{-1}$ (-1.77 ppm $m^{-1}$) at sunset to 0.015 K $m^{-1}$ (-0.69 ppm $m^{-1}$) at sunrise between 5 (4) and 25 (24) m.

In the evening transition (18:00-20:00 LT), a shallow stable daytime layer within the canopy was present (González-Armas et al., 2025). Over time, atmospheric stratification in the canopy layer weakens, mixing the atmosphere. Eventually, a shallow well-mixed layer (5 to 25 m) developed during the morning transition (04:00-06:00 LT) just before sunrise. We hypothesise that the mixing within the canopy layer originates from the cold layer forming on top of the canopy following the strong longwave radiative cooling. When the cooling was sufficiently strong, cold air sank downward into the canopy, mixing the atmosphere below. According to a study by Santos et al. (2016), mixing by sinking cold air is possible with radiative cooling rates $\leq$ -40 W $m^{-2}$, we observed that the threshold was met during most of the nights during the CloudRoots campaign (not shown). In addition, we observed a positive heat flux ($\overline{w'\theta'}$) during S2, S3, S4 and W3 within the canopy layer, which potentially is related to the downward movement of cold air (w'$<0$ & $\theta$'$<0$) (Appendix B).

Regardless of the observed temporal pattern within the canopy, we must acknowledge the large variability between the nights. The standard deviations of the $\theta$ profiles are largest during the evening transition (18:00-22:00 LT). The large deviations are thought to originate from strong cooling during the evening transition (Stull, 1988), explaining the relatively large hourly variation (black error bars) compared to later in the night. For $CO_2$, the largest standard deviation in the evening transition was

https://doi.org/10.5194/egusphere-2026-684
Preprint. Discussion started: 17 February 2026


observed at 4 m, mainly due to variation in $CO_2$ across the nights (red error bars). The large variability between nights can result from two mechanisms: 1) the strength of the stable stratification, which prevents mixing, and 2) the absolute temperature during the day. The latter is important because soil respiration increases with temperature (Lloyd and Taylor, 1994), as is confirmed by the highest observed $CO_2$ variability at 4 m. During daytime, $CO_2$ respired by the soil is unable to vertically ascend in the stable layer (González-Armas et al., 2025). In addition, the main uptake of $CO_2$ during the day happened in the canopy crown ($\pm$ 24 m), enhancing the daily $CO_2$ gradient in the canopy layer. After the evening transition, the stable layer within the canopy disappeared and the $CO_2$ molar fraction increased, especially at 24 m. The increase at 24 m can be caused not only by nighttime respiration of vegetation but also by $CO_2$ mixing upward from the surface.

After midnight, we observed that standard deviations increased above the canopy for both $\theta$ and $CO_2$, which we attributed to differences in exchange between strongly and weakly stable regimes. Increased mixing between the two layers in the weakly stable regime redistributed $CO_2$ from the canopy layer to the stable layer above, whereas it does not during the strongly stable regime. The largest standard deviations in $CO_2$ vertical profiles, at all heights, occur in the morning transition (04:00-06:00 LT). It is hypothesised that the profiles at 06:00 LT are influenced by the enhanced mixing during the morning, as the first solar radiation reaches the surface by 06:00 LT. In a previous study by Dupont et al. (2024), they found that the evolution of $CO_2$ in the early morning differs between low and high wind speeds. The different wind speeds (Fig. 5c) in our two regimes may explain the large contrast between nights during the morning transition.

### 3.2.1 Coupling between the canopy-atmosphere interface

In Fig. 4, we present the temporal evolution of $Ri_{atm}$ and $Ri_{can}$ for the average of the 11 nights, one more turbulent night (strongly stable: 10-11 August) and one less turbulent night (weakly stable: 18-19 August). In Fig. 4, $Ri_{atm}$ increased during the night for all three cases. However, it increased most significantly in the strongly stable night. In the weakly stable night, the $Ri_{atm}$ remained below $\mathrm{Ri}_c$ throughout the night, indicating continuous turbulence. Contrary to $Ri_{atm}$, $Ri_{can}$ decreased over time. For the mean and strongly stable night, $Ri_{can}$ decreased towards the end of the night (only visible between 04:00-06:00 LT due to low wind speeds). Note that it never reaches $Ri_c$ due to the stable gradient between 25 m and 35 m (Fig. 3), which we included because $Ri_{can}$ becomes unstable if we only include the profile below 25 m, where the windspeed approaches zero. In the weakly stable night, $Ri_{can}$ decreased between 22:00-02:00 LT, indicating significant mixing between the stable and canopy layer, also observed in Santos et al. (2016). Interestingly, the $Ri_{can}$ for the weakly stable night increased towards the end of the night, likely due to mixing; the $\theta$ gradient over height is too weak at the canopy top, preventing the sinking motion of cold air.

Based on the findings above, we discuss the degree of coupling of the canopy and atmospheric layers. De Kauwe et al. (2017) proposed a decoupling parameter that describes the strength of decoupling of the two layers. With our results, we were able to roughly estimate a decoupling factor based on the $Ri_{atm}$ and $Ri_{can}$. We found the two layers to be decoupled if $Ri_{atm} > Ri_c$ and $Ri_{can} < Ri_c$ and coupled if $Ri_{atm} < Ri_c$ resulting in $Ri_{can} > Ri_c$ at the end of the night. When we apply our simple decoupling parameter to our strongly and weakly stable profiles in Fig. 5e, we indeed find that the strongly stable profile is decoupled. In contrast, the weakly stable profile is coupled, allowing interactions between the two layers. The

https://doi.org/10.5194/egusphere-2026-684
Preprint. Discussion started: 17 February 2026


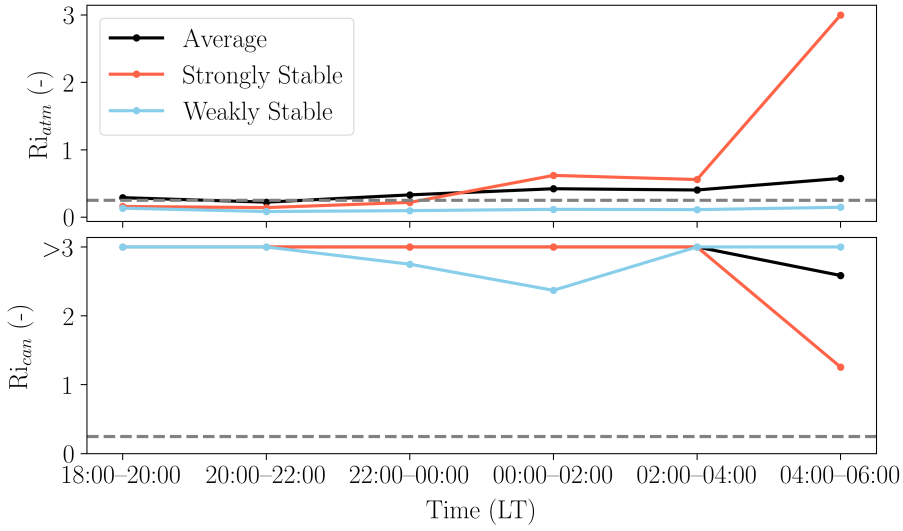


**Figure 4.** Two-hour average temporal evolution of the Richardson number above canopy (top) and Richardson number below canopy (bottom). Where the black line is the average of 11 studied nights, the red line represents the strongly stable profile from the night of 10-11 August 2022 and the blue line the weakly stable night on the night of 18-19 August 2022. The striped grey line indicates the critical Richardson number (0.25).

difference between the two regimes controls the build-up of $CO_2$ below the canopy, and thus the magnitude of the flux when the turbulence suddenly increases (Acevedo et al., 2016).

### 3.3 Exchange of $CO_2$ and heat at the canopy-atmosphere interface

We evaluated the governing equations of $TKE$ (Section 3.3.1), heat (Section 3.3.2) and $CO_2$ (Section 3.3.3) only with the periods classified as strongly and weakly stable (Table 2). To understand the basic characteristics of these periods, we show in Fig. 5 the average vertical profiles of $\theta$, $CO_2$, $U$, Ri, $TKE$ and $u_*$ for the selected periods of the strongly and weakly stable (Table 2). By inspecting the vertical profiles of $\theta$ (Fig. 5a), we found that the strongly stable vertical $\theta$ profile shows a larger temperature gradient between 25 and 50 m (2.08 K) than the weakly stable profile (1.29 K). For $CO_2$ (Fig. 5b), a similar pattern is observed: the $CO_2$ gradient between 38 and 79 m is larger for the strongly stable regime (-21.8 ppm) than during the weakly stable regime (-5.5 ppm). The observed differences between the strongly and weakly stable vertical profiles (Fig. 5ab) are partly explained by the influence of the temporal evolution on $\theta$ and $CO_2$ during the night. However, we believe that turbulent mixing during the weakly stable periods also partly explains the difference between the profiles.

Wind speed variation with height generates shear and mixes the stable layer; this clearly differs between the strongly and weakly stable profiles (Fig. 5c). Already at 25 m, the wind speed and gradient with height in the weakly stable cases are enhanced, compared to the strongly stable profile. At 50 m, the threshold of 2.5 m $s^{-1}$ is reached in the weakly stable profile, but not for the strongly stable profile. In addition, we observe that in the weakly stable regime, the increased $U$ results in 0.2

https://doi.org/10.5194/egusphere-2026-684
Preprint. Discussion started: 17 February 2026


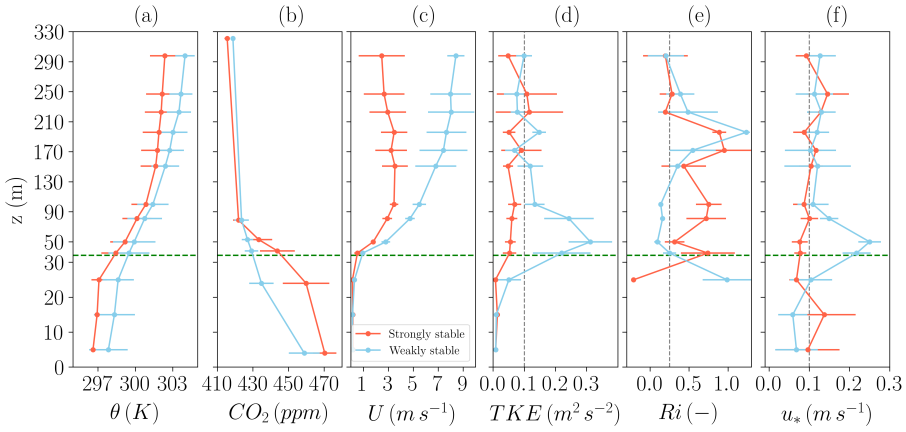


**Figure 5.** Vertical profiles above and below the canopy, the dashed green line indicates the aerodynamic top of the canopy (32 m). Profiles are shown for a) potential temperature ($\theta$), b) $CO_2$, c) wind speed ($U$), d) turbulent kinetic energy ($TKE$), e) Richardson number ($Ri$) and f) friction velocity ($u_*$). In the figure, the red line shows the average of the strongly stable cases, with the standard deviation in error bars. The blue lines show the same, but for the weakly stable cases. The vertical lines in c, d, e and f represent the threshold values (at 50 m) used to select the strongly and weakly stable profiles, being 2.5 m s$^{-1}$, 0.1 m$^2$ s$^{-2}$, 0.25 and 0.1 m s$^{-1}$ respectively.

m$^2$ s$^{-2}$ $> TKE >$ 0.4 m$^2$ s$^{-2}$, $Ri < Ri_c$ and 0.2 m s$^{-1}$ $>$ u$_*$ $>$ 0.3 m s$^{-1}$ at 50 m (Fig. 5def). For the strongly stable regime, the wind remained below 2.5 m s$^{-1}$ at 50 meters, resulting in the low $TKE <$ 0.1 m$^2$ s$^{-2}$, $Ri > Ri_c$ and u$_*$ $<$ 0.1 m s$^{-1}$ at 50 m, similar to the results of Dias-Júnior et al. (2017). Above 200 m, we observe that the TKE, $Ri$ and u$_*$ no longer show large differences between the two regimes, indicating that the regime has no significant influence on the residual layer.

### 3.3.1 Observational interpretation of the $TKE$ budget

We evaluated the terms of the $TKE$ budget (Eq.3) one by one, distinguishing between the strongly and weakly stable profiles above (Fig. 6). In Fig. 6, the average logarithmic fitted profiles are plotted for the strongly and weakly stable regimes. The shaded area indicates the standard deviation between the four selected periods.

For both the strongly and weakly stable regimes, the $TKE$ tendency (Fig. 6a) is 10-100x smaller compared to the individual terms and shows no significant difference between the regimes. The buoyancy term (Fig. 6b) is most negative at the canopy top and increases with height. For the weakly stable regime, buoyancy is more negative (-1.70 x $10^{-3} \pm$ 0.94 x $10^{-3}$ m$^2$ s$^{-3}$) than for the strongly stable regime (-0.30 x $10^{-3} \pm$ 0.31 x $10^{-3}$ m$^2$ s$^{-3}$), indicating, that there is almost no vertical turbulent movement in the strongly stable regime. The shear term at the canopy top (Fig. 6c), is significantly larger for the weakly stable regime (6.20 x $10^{-3} \pm$ 2.05 x $10^{-3}$ m$^2$ s$^{-3}$) than for the strongly stable regime (0.16 x $10^{-3} \pm$ 0.52 x $10^{-3}$ m$^2$ s$^{-3}$). This is in accordance with Mironov and Sullivan (2016), who found that the magnitude of shear is about three times larger than buoyancy in the weakly stable regime.

https://doi.org/10.5194/egusphere-2026-684
Preprint. Discussion started: 17 February 2026


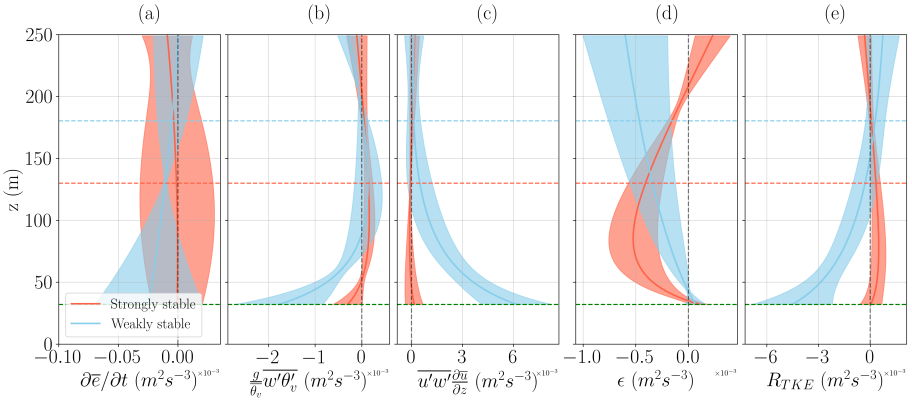


**Figure 6.** Conservation of turbulent kinetic energy (TKE), according to Eq.4. Here the red line represents the average of the strongly stable profiles and the shaded area, the standard deviation. Blue is the same, but for the weakly stable profiles. The graphs represent the terms of the $TKE$ equation: a) the $TKE$ tendency, b) the buoyant consumption, c) the shear production, d) dissipation and e) the residual. The horizontal lines indicate the average $h_{NBL}$, calculated for the strongly (red) and weakly (blue) stable regimes.

Dissipation below $h_{NBL}$ is more important for the strongly stable regime (Fig. 6d). These results are different from Stull (1988), which reports dissipation to be highest when most turbulence is present. In addition, Mironov and Sullivan (2016) reports dissipation to have the same magnitude as shear minus buoyancy. To understand why our approximation differs, it is vital to understand the effect of forest canopies on the production and destruction of TKE. The canopy generates increased shear compared to bare soil and grassland, due to the higher surface roughness of its porous surface (Khanna and Medvigy, 2014). Within the canopy crown, increased dissipation caused by the canopy drag (Dwyer et al., 1997) results in a layer of net dissipation (Chen and Chamecki, 2023). To balance the production of shear above the canopy and dissipation in the canopy, downward transport of $TKE$ becomes important in the stable forest layer (André et al., 1978; Vickers and Thomas, 2013; Science Panel for the Amazon., 2021). In our calculations, we used mean values to estimate the dissipation. Therefore, our calculations do not correct for these effects and are a simplification of reality. In future studies, the dissipation can be improved by using a method based on spectra and the Kolmogorov theory, which was beyond the scope of this study. However, considering the parameterisation, we can explain our results. We explain the results by a stronger temperature gradient in the strongly stable atmosphere (Fig. 5a), which decreased $\lambda$ from $\pm$ 10 m in the weakly stable atmosphere to $\pm$ 2 m in the strongly stable atmosphere. In our parameterisation, dissipation is negatively correlated to $\lambda$, causing an increase in the strongly stable atmosphere. Above $h_{NBL}$, dissipation is more important in the weakly stable regime: here, the temperature gradient has disappeared, making dissipation mainly dependent on the windspeed, which is enhanced in the weakly stable atmosphere (Fig. 5c).

Finally, a relatively large residual (Fig. 6e) remains in the weakly stable atmosphere (4.51 x $10^{-3} \pm 2.33$ x $10^{-3}$ $m^2$ $s^{-3}$). A large part of the residual can be explained by the simplification of dissipation. Additionally, advection and pressure fluctuations become important in the canopy layer and 20-30 m above in the stable atmosphere (Chen and Chamecki, 2023). Advection is

https://doi.org/10.5194/egusphere-2026-684
Preprint. Discussion started: 17 February 2026


found to be negative over crests and positive over troughs in the landscape (Chen and Chamecki, 2023), since ATTO is located on a crest, negative horizontal advection is expected. For the strongly stable regime, the residual is small (0.04 x $10^{-3}$ $\pm$ 0.64 x $10^{-3}$ $m^2$ $s^{-3}$ at the canopy top) (Fig. 6e), and is attributed to the measuring and calculation errors.

### 3.3.2 Observation interpretation of the heat budget

Secondly, we evaluated the governing equation of heat, which quantifies the heating of the atmosphere as a function of the turbulent transport of heat (driven by shear), radiative cooling and other processes represented by the residual. The average results for the selected periods are shown in Fig. 7. The temperature tendency is negative for both the strongly (-0.29 $\pm$ 1.06 K $h^{-1}$ at the canopy top) and weakly (-0.37 $\pm$ 0.49 K $h^{-1}$ at the canopy top) stable regime (Fig. 7a). However, especially in the strongly stable regime, the temperature tendency has a large standard deviation, caused by the variation in the temperature tendency between S1, S2, S3 and S4. Above the canopy, at 50 m, the temperature decreased during S2 (-1.7 K $h^{-1}$) and S4 (-0.03 K $h^{-1}$) but increased during S1 (0.3 K $h^{-1}$) and S3 (0.3 K $h^{-1}$). Two processes can cause the increase in temperature: 1) non-turbulent sub-mesoscale effects in strongly stable periods (Oliveira et al., 2018), and 2) the presence of the NLLJ during S3 and S4 potentially caused the mixing of air from above, increasing the temperature (Smedman, 1988; Mahrt, 1998; Karipot et al., 2006).

The second term, turbulent transport of heat, decreases logarithmically with height during the night (Fig. 7b). The weakly stable profile showed more negative turbulent transport of heat (-3.62 $\pm$ 1.54 K $h^{-1}$) at the canopy top, compared to the strongly stable profile (-1.23 $\pm$ 0.79 K $h^{-1}$). The difference can be explained by enhanced shear in the weakly stable regime, which increased transport of cold air from within the canopy to aloft. Turbulent transport of heat above the canopy top in the weakly stable profiles is up to 2 K $h^{-1}$ higher, as for the grass surface (Stull, 1988). A possible explanation could be the increased surface roughness of the trees, which enhanced turbulence. As expected, when we move up towards the neutral residual layer, above $h_{NBL}$, turbulent heat transport approaches zero.

Radiative cooling decreases logarithmically with height above the canopy top (Fig. 7c). The strongly stable regime (-0.35 $\pm$ 0.02 K $h^{-1}$ at the canopy top) shows higher radiative cooling than the weakly stable regime (-0.24 $\pm$ 0.35 K $h^{-1}$ at the canopy top). The presence of clouds during the selected periods of W1 and W2 likely decreased radiative cooling (Appendix C). However, the cooling is small compared to the values reported in Stull (1988) where they found radiative cooling of -2 K $h^{-1}$ at the cooling surface. The lower cooling is explained by the non-homogeneous canopy surface, where the most intense cooling occurred within the canopy, where the leaf density is highest.

Similar to the governing equation of TKE, a large residual remained in the governing equation of heat. The positive residual is attributed to the heterogeneous temperature pattern observed in the Amazon rainforest. At 50 m, where the residual is 0.74 $\pm$ 0.62 K $h^{-1}$ for the strongly stable case and 1.75 $\pm$ 0.40 K $h^{-1}$ for the weakly stable case, temperature advection may explain the residual. A horizontal temperature gradient of 0.15 K $km^{-1}$ downwind would already lead to a heat advection of about 1.0 K $h^{-1}$ in the strongly stable regime and 1.6 K $h^{-1}$ in the weakly stable regime. Multiple processes can initiate horizontal temperature differences in the Amazon rainforest, for example, differences in land use or soil moisture content (Al-Kayssi

https://doi.org/10.5194/egusphere-2026-684
Preprint. Discussion started: 17 February 2026


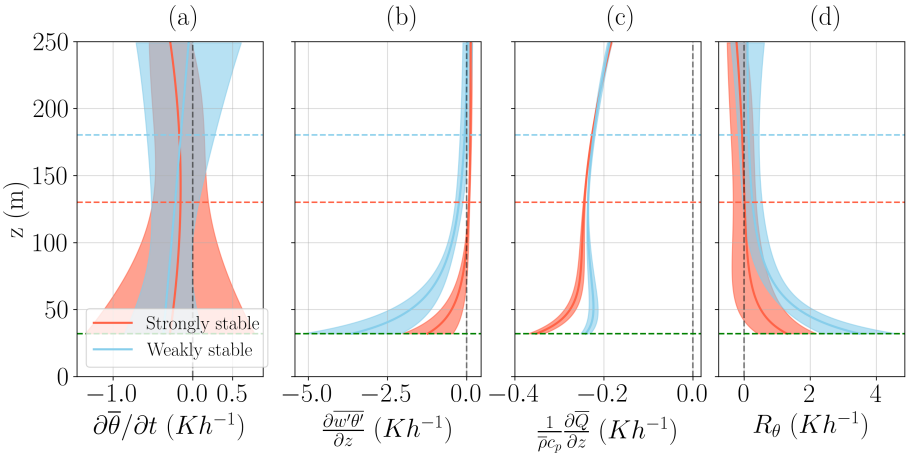


**Figure 7.** Conservation of heat, according to the simplified form of Eq. 4. Here the red line represents the average of the strongly stable profiles and the shaded area is the standard deviation. Blue is the same, but for the weakly stable profiles. The graphs represent the terms of the heat equation: a) the temperature tendency, b) the turbulent transport of heat, c) radiative heating and d) the residual. The horizontal lines indicate the average $h_{NBL}$, calculated for the strongly and weakly stable regimes.

et al., 1990; Gash and Nobre, 1997). To the east (main wind direction) of the ATTO, a swampy area is located, which likely increased nocturnal temperatures there; this may explain the positive residual.

### 3.3.3 Observational interpretation of the $CO_2$ budget

Finally, we evaluated the governing equation of $CO_2$. The terms of the governing equation of $CO_2$ are depicted per term in Fig. 8 and are described one by one in this section. For the $CO_2$ tendency (Fig. 8a), we observe that the $CO_2$ tendency is positive (1.62 $\pm$ 1.96 ppm $h^{-1}$ at the canopy top) for the weakly stable regime ($CO_2$ increasing over time) and negative (-5.61 $\pm$ 8.23 ppm $h^{-1}$ at the canopy top) for the strongly stable regime. The increase in $CO_2$ for the weakly stable regime can be caused by coupling between the top of the canopy layer and the stable layer above, enabling mixing of $CO_2$-enhanced air from within the canopy upward. Two processes can cause the decrease in $CO_2$ during the strongly stable period: 1) the NLLJ mixing $CO_2$-depleted air downwards (Smedman, 1988; Mahrt, 1998; Karipot et al., 2006) and 2) drainage of $CO_2$ at the surface (Goulden et al., 2006; de Araújo et al., 2010). The drained air at the surface is replaced by subsiding $CO_2$-depleted air from above, decreasing the $CO_2$ concentration. However, we must consider the variation in the tendency, especially during the strongly stable regime. The large variation is caused by S3 (Table 2), which shows an increase instead of a decrease in $CO_2$ over time. The increase of $CO_2$ in S3 (7.1 ppm $h^{-1}$ at the canopy top) is related to the period of intermittent turbulence before S3 (Acevedo et al., 2008). Because a large timeframe of 30 min was used for the tendency calculation, the period with increased mixing significantly influenced the $CO_2$ tendency.

For the turbulent transport of $CO_2$, we observed that on average the weakly stable regime has a higher turbulent transport of $CO_2$ (33.94 $\pm$ 37.45 ppm $h^{-1}$ at the canopy top) than the strongly stable regime (23.39 $\pm$ 9.54 ppm $h^{-1}$ at the canopy top).

https://doi.org/10.5194/egusphere-2026-684
Preprint. Discussion started: 17 February 2026


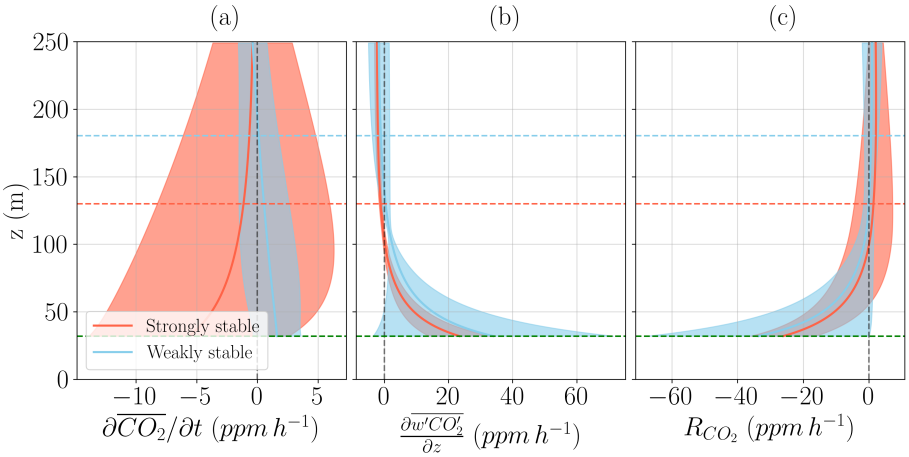


**Figure 8.** Conservation of $CO_2$, according to the simplified form of Eq. 5. Here, the red line represents the average of the strongly stable profiles, and the shaded area is the standard deviation. Blue is the same, but for the weakly stable profiles. The graphs represent the terms of the $CO_2$ equation: a) the $CO_2$ tendency, b)the Turbulent transport of $CO_2$ and c) the residual. The horizontal lines indicate the average $h_{NBL}$, calculated for the strongly and weakly stable regimes.

However, the standard deviation of the turbulent transport of $CO_2$ is large for the weakly stable regime. The large standard deviation is caused by W3 and W4, which showed small turbulent transport of $CO_2$ ($\pm$ 3 ppm $h^{-1}$ at 50 m) because of the limited divergence of the $CO_2$ flux between 50 and 81 m, indicating the presence of turbulence up to higher levels in the atmosphere, as the magnitude of the fluxes at 50 m was similar to W1 and W2. In contrast, W1 and W2 showed significant amounts of turbulent transport ($\pm$ 15 ppm $h^{-1}$ at 50 m) between the canopy and stable layer. The influence of shear on $CO_2$ transport is also observed during the day (Moonen et al., 2025). During the daytime, canopy ejections of $CO_2$ are found to have a significant contribution to the daily carbon flux. To determine whether nocturnal $CO_2$ fluxes are significant for the carbon balance during the night, we calculated $CO_2$ fluxes at 50 m during weakly stable periods. During the four weakly stable hours, we observed an average $CO_2$ flux at 50 m of 3.82 $\mu$mol $m^{-2}$ $s^{-1}$, here the highest flux found was 6.38 $\mu$mol $m^{-2}$ $s^{-1}$ during W2. These observations confirmed that the $CO_2$ turbulent fluxes measured above the canopy are significant in the night (Culf et al., 1997; Mahrt, 2011; Oliveira et al., 2013, 2018). In contrast, during the decoupled strongly stable regime, we observed an average $CO_2$ flux at 50 m of only 0.16 $\mu$mol $m^{-2}$ $s^{-1}$.

Similar to $TKE$ and heat, the residual is significant for the conservation equation of $CO_2$. The negative residual (Fig. 8c) suggests a negative source of $CO_2$ at ATTO. During the CloudRoots campaign, aeroplane measurements were taken at 9:00 and 13:00 LT on the morning of the 18th of August. The lowest measuring level by the plane was 200 m, at 200 m height, a heterogeneous $CO_2$ pattern was observed (de Feiter et al., 2025). The measurement time was after sunrise; however, 9:00 LT is still in the morning transition, according to Henkes et al. (2021), suggesting that the mixed layer was not completely developed at 9:00 LT. East of the ATTO, we observed an area depleted in $CO_2$, resulting in a $CO_2$ gradient of about -0.68 ppm $km^{-1}$ from the depleted area to ATTO. The $CO_2$ gradient and measured windspeed lead to an estimated advection term of about -6

https://doi.org/10.5194/egusphere-2026-684
Preprint. Discussion started: 17 February 2026


ppm $h^{-1}$ at 50 m, explaining a large part of the residual at 50 m ($\pm$ 10 ppm $h^{-1}$). At the canopy top, the observed $CO_2$ molar fraction likely is higher, due to the logarithmic nocturnal profile (Fig. 5b). The higher magnitude of $CO_2$ suggests larger $CO_2$ advection close to the canopy top. Additionally, during the night, the advection could be higher because of morning mixing, which decreases the $CO_2$ molar fractions in the atmosphere.

## 4 Discussion

The CloudRoots measuring campaign enabled us to provide an in-depth description of the dry season NBL above the Amazon rainforest. However, we must consider that our dataset only covered two weeks. From these two weeks, we could only select eight hours, for which all six of our strict criteria applied, to determine whether the period belonged to the strongly or weakly stable regime (Table 1). Only these eight hours were used to evaluate the governing equations. These limitations illustrate how non-stationary the NBL is in the Amazon.

With the temporal limitations in mind, we want to emphasise the following three points of discussion: (1) the reliability of nocturnal data, (2) the influence of daytime clouds on nighttime conditions, and vice versa, concluding with (3) recommendations for future research. However, for all discussion points, we have to acknowledge the uncertainty in our research due to the assumptions we had to make to interpret and quantify with observations the TKE, heat and $CO_2$ equations. In our resulting residual terms, we find that horizontal heterogeneity is crucial to consider in the Amazon NBL. This complicates the implications of our findings to other areas in the Amazon rainforest and stresses the importance of measuring horizontal terms and the complexity of nocturnal observations.

### 4.1 Reliability of nocturnal data

Eddy covariance measurements in general, and thus also the data collected during the CloudRoots campaign, are challenging to use during the night (Loescher et al., 2006; Aubinet, 2008). With eddy covariance devices, the turbulent transport of momentum, heat and $CO_2$ by eddies is measured. In a strongly stable NBL, these eddies are small and only reach limited heights. In addition, the decoupling of the canopy and stable layer aloft caused by the stable stratification prevents the movement of eddies between the two layers. Consequently, there is no $CO_2$ exchange between the canopy layer and stable layer aloft, resulting in $CO_2$ being stored in the canopy layer, and the measured carbon flux on top of the canopy often underestimates the total carbon flux (Goulden et al., 1996; Culf et al., 1999; Aubinet et al., 1999; Lloyd et al., 2007). It is therefore likely that our estimated $CO_2$ flux is an underestimation of the total flux, especially during the strongly stable regime. To obtain reliable estimations of the nighttime $CO_2$ flux, we recommend that future studies include storage of $CO_2$ in the canopy. González-Armas et al. (2025) estimated the morning storage flux using vertical observations from CloudRoots. The paper found that including $CO_2$ storage improved the correlation between observed and modelled net ecosystem exchange during the morning transition, stressing the importance of nocturnal $CO_2$ storage for the daily carbon flux.

https://doi.org/10.5194/egusphere-2026-684
Preprint. Discussion started: 17 February 2026


### 4.2 Influence of clouds

In this study, we only used the cloud measurements from the campaign to discuss the possible effect of clouds on radiative cooling. However, the earlier identified cloud regimes, shallow convective and shallow to deep convective (Vilà-Guerau de Arellano et al., 2024), will likely influence the evolution of the nights, and the night itself might influence cloud formation, during the morning transition and next day (Henkes et al., 2021; Dupont et al., 2024). Additionally, clouds influence atmospheric radiative transfer, which will influence the radiative cooling and thus the formation of the NBL. For example, during the night of 12-13 August, clouds were observed after sunset (Appendix C); radiative cooling at sunset decreased, limiting the formation of the NBL during the first hours of the night.

Furthermore, the influence of (nocturnal) clouds on trace gases remains poorly understood and has only been evaluated in a few studies. Machado et al. (2024), observed that during the night the $CO_2$ molar fraction in the atmosphere decreases after a rainfall event, which was correlated with increased humidity, decreased temperature and radiation. Other studies, which relate clouds and $CO_2$ fluxes, are mainly limited to daytime conditions. Moonen et al. (2025) analysed small-scale processes associated with wind gusts driven by the presence of clouds, and found a weak influence of the clouds on the $CO_2$ exchange between the canopy and directly aloft. Mendonça et al. (2023) found that deep convective clouds cause strong wind gusts, locally causing tree mortality and strong $CO_2$ ejections. Finally, de Feiter et al. (2025) found that shallow daytime clouds play an important role in ventilating $CO_2$ from the boundary layer by de Feiter et al. (2025). The importance of the daytime clouds suggests that, also during the night, clouds could have a significant role in $CO_2$ exchange. Therefore, future research should try to extend these findings to nocturnal conditions.

### 4.3 Future recommendations

We believe, based on this study, that future research should be focused on high-resolution canopy-atmosphere-cloud observations (Vilà-Guerau de Arellano et al., 2023), measuring with a duration of multiple seasons. It is crucial to extend the measurements beyond the dry season because of the significant difference in turbulence regimes during the seasons (Mendonça et al., 2023). In addition, high-resolution measurements are vital to observe the sinking motions of cold air into the canopy. We did not observe an atmospheric layer around 25 m, significantly colder than below, only an increased heat flux (Appendix B) and a well-mixed layer at the end of the night. However, the layer may be present, as it may be only a few meters thick and not captured with the current vertical measurement resolution. Therefore, measurements of the upward and downward LWR and temperature with small high vertical resolution ($\pm$ 1 m) in the radiative cooling layer (20-30 m) are advised for future research. These measurements would also make it possible to validate the RTE+RRTMGP model output with observations, providing more confidence in our radiative cooling estimate and the results of the radiation model in general.

Finally, these observational studies could help us to bridge the gap between one-layer and multilayer canopy models (Bonan et al., 2021). The advancement to multi-layer canopy models is crucial due to increasing model resolution, but even so, to improve model parameterisations in large-scale models. The high-resolution vertical observations of great importance for validating state-of-the-art, multi-layer canopy models using large-eddy simulation techniques (Ma and Liu, 2019; Pedruzo-

https://doi.org/10.5194/egusphere-2026-684
Preprint. Discussion started: 17 February 2026


Bagazgoitia et al., 2023). These models have already proven to yield important improvements in canopy-atmosphere interactions. Therefore, we think the multilayer canopy models are the next step in improving the complex nocturnal vegetation-atmosphere interactions. However, to do so, it is vital to understand the dynamics and radiative properties of the NBL both within and above the canopy.

## 5 Conclusions

This study aimed to enhance our understanding of the processes that drive NBL characteristics by thoroughly analysing observations collected during the CloudRoots campaign. We investigated the dynamic and radiative characteristics of the NBL in the Amazonian dry season, focusing on the exchange of $CO_2$ and heat from within the canopy to aloft. We were able to quantify the exchange by utilising observations to evaluate the governing equations of TKE, heat and $CO_2$, which clearly describe the contribution of shear and radiative cooling. With the equations, we emphasised the difference in exchange between the strongly and weakly stable regimes. The detailed characterisation was possible using vertical profiles measured at ATTO, during the CloudRoots campaign in the dry season of 2022 (8-21 August). Above the canopy, we observed a stable layer formed by the radiative cooling at the canopy top. The stable stratification was confirmed by the shallow $h_{NBL}$ between 150 and 188 m during the nights of the campaign. However, we observed a large variation in $h_{NBL}$ caused by the non-dominance of either shear or radiative cooling throughout one night. This resulted in interchanging periods dominated by shear (weakly stable), resulting in high $h_{NBL}$ ($\pm$ 180 m) and periods dominated by radiative cooling (strongly stable), associated with low $h_{NBL}$ ($\pm$ 130 m). The layer within the canopy transforms from stable at the beginning of the night to well-mixed at the end of the night. Well-mixed profiles are most pronounced in the strongly stable nights, where limited shear was unable to mix the two layers. Limited-presence of shear caused the formation of a strongly stratified layer, which initiated the sinking motion of the cold air downward from the canopy top, mixing the canopy layer.

The exchange of $CO_2$ between the within and above canopy atmosphere was found to be mainly governed by shear; radiative cooling had a limited direct influence on the exchange. In the strongly stable periods, the shear production was small, leading to limited turbulent exchange of $CO_2$ from the canopy upward (19.74 $\pm$ 8.11 ppm $h^{-1}$) and heat (-1.23 $\pm$ 0.79 K $h^{-1}$) between the canopy and the stable layer. In contrast, during the weakly stable periods, increased shear at the canopy top enhanced exchange of $CO_2$ (29.13 $\pm$ 31.75 ppm $h^{-1}$) and heat (-3.62 $\pm$ 1.54 K $h^{-1}$). The increased $CO_2$ exchange in the weakly stable regimes confirms the coupled state of the canopy layer and atmosphere aloft. The coupling makes significant $CO_2$ fluxes of 3.52 $\mu$mol $m^{-2}$ $s^{-1}$ possible. In contrast, canopy-atmosphere interactions are inhibited in the decoupled strongly stable regime, leading to a $CO_2$ flux of only 0.16 $\mu$mol $m^{-2}$ $s^{-1}$. The difference between the regimes is governed by a myriad of processes happening both within the canopy, aloft of the canopy and between the two layers. With this we highlight the importance of taking into account both the within-canopy and above-canopy layers to study nocturnal $CO_2$ exchange at the canopy-atmosphere interface in dense forest canopies like the Amazon rainforest.

https://doi.org/10.5194/egusphere-2026-684
Preprint. Discussion started: 17 February 2026


## Appendix A: ERA5 and RTE+RRTMGP compared to tower observations

Figure A1 depicts ERA5 observations compared to tower observations of one selected strongly stable hour (S1) and one selected weakly stable hour (W1). The remaining selected hours in Table 2 are comparable to the two comparisons shown. We find that for S1, the temperature profiles of ERA5 and the tower are very similar. However, below the canopy, the difference between the model and observations increases (max 2 K). The volume moisture ratio (vmr) of S1 has an error of approximately 0.001 ppmv, but follows the same trend as observations. For W1, the ERA5 and tower observations are less similar. The error in temperature above the canopy has a maximum of 1.8 K, while the error below the canopy is similar to S1. The vmr of W1 has an error of approximately 0.004 ppmv at the canopy top, but decreases towards $h_{NBL}$.

Figure A2 depicts the RTE+RRTMGP model outcomes of upward and downward longwave radiation (Top) and resulting net radiation (Bottom), compared to the observations at 75 m. The difference between model and observations is smallest for the upward longwave radiation (max 3.3 W $m^{-2}$), and of similar magnitude for the downward (max 12.3 W $m^{-2}$) and net radiation (max 11.5 W $m^{-2}$).

## Appendix B: Measured Eddy Covariance Fluxes of Heat and $CO_2$ Fluxes

The heat flux (Fig. B1) is plotted below for the selected periods for the strongly and weakly stable periods. We observe that in S2, S3 and S4 the heat flux increases below the canopy, indicating downward transport of cold air. In the weakly stable atmosphere, the opposite happens; here, the heat flux becomes negative above the canopy, indicating upward motion of cold air.

## Appendix C: Cloud Observations and Net Longwave Radiation

Cloud observations from the MIRA radar, during the nights from which the strongly and weakly stable profiles were selected, are plotted in Fig. C1. The blue Shallow cumulus (SCu) clouds around the top of the residual layer were found to be caused by high moisture areas. On the night of 12-13 August (the night of S3 & S4), the MIRA radar observed some Cirrus (Ci) and Alto stratus (As) clouds roughly 2 hours after sunset and before sunrise. On the night of 13-14 August (night of W1 & W2), Ci and Cirrostratus (Cs) clouds were observed by the MIRA radar until midnight.

*Author contributions.* Anna C. Huitema: Writing – review & editing, Writing – original draft, Visualisation, Validation, Methodology, Investigation, Formal analysis. Vincent S. de Feiter: Writing – review  editing, Writing - original draft, Supervision, Methodology, Investigation, Formal analysis, Data curation. Raqel Gonzáles-Armas: Writing – review & editing, Supervision, Methodology, Investigation, Formal analysis, Data curation. Oscar Hartogensis: Writing – review & editing, Project administration, Funding acquisition. Hella van Asperen: Writing – review & editing, Resources, Data curation. Cléo Quaresma Dias-Júnior: Writing – review & editing, Resources, Data curation. Jordi

https://doi.org/10.5194/egusphere-2026-684
Preprint. Discussion started: 17 February 2026


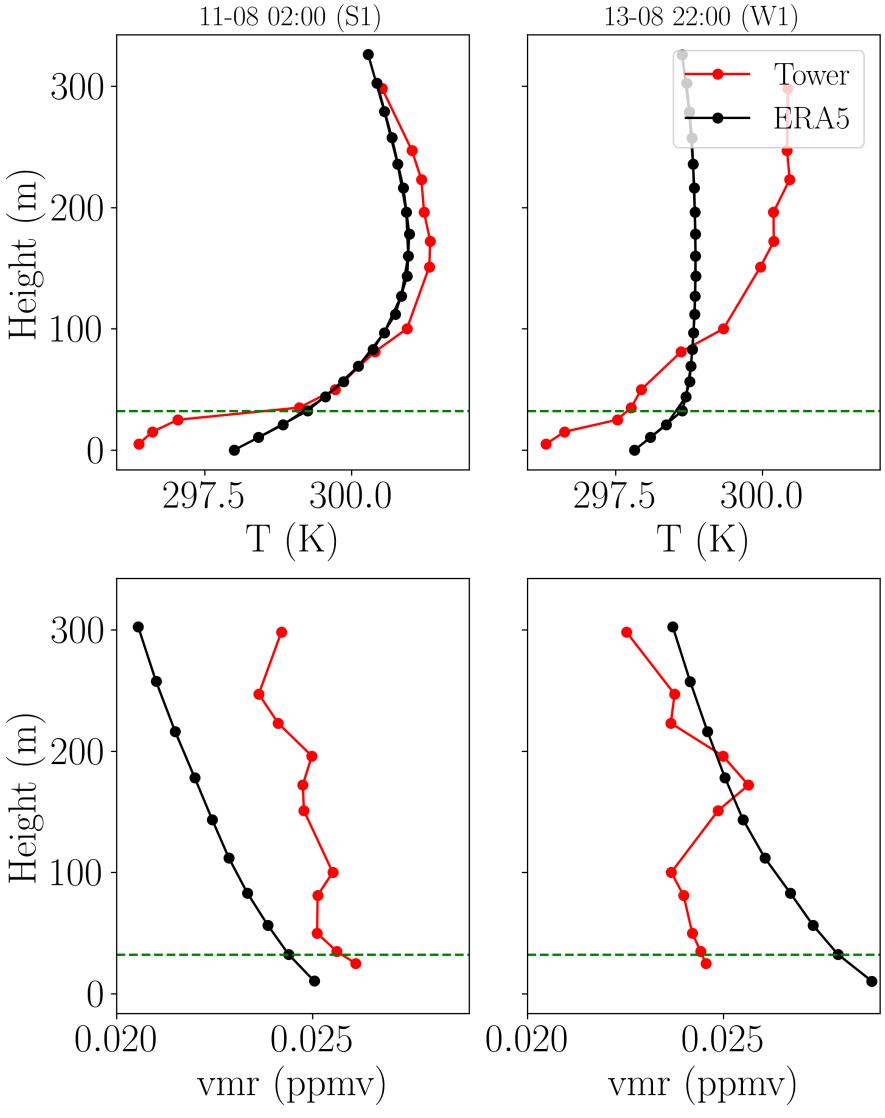


**Figure A1.** ERA5 vertical profiles (Black) of temperature (top) and volume moisture ratio (vmr) (bottom) compared to tower observations (red). The vertical profiles are from one strongly stable hour (S1) and one weakly stable hour (W1)

Vilà-Guerau de Arellano: Writing – review & editing, Visualisation, Supervision, Resources, Project administration, Investigation, Funding acquisition, Conceptualisation.

*Competing interests.* The authors declare that they have no financial or personal interest relevant to this study.

https://doi.org/10.5194/egusphere-2026-684
Preprint. Discussion started: 17 February 2026


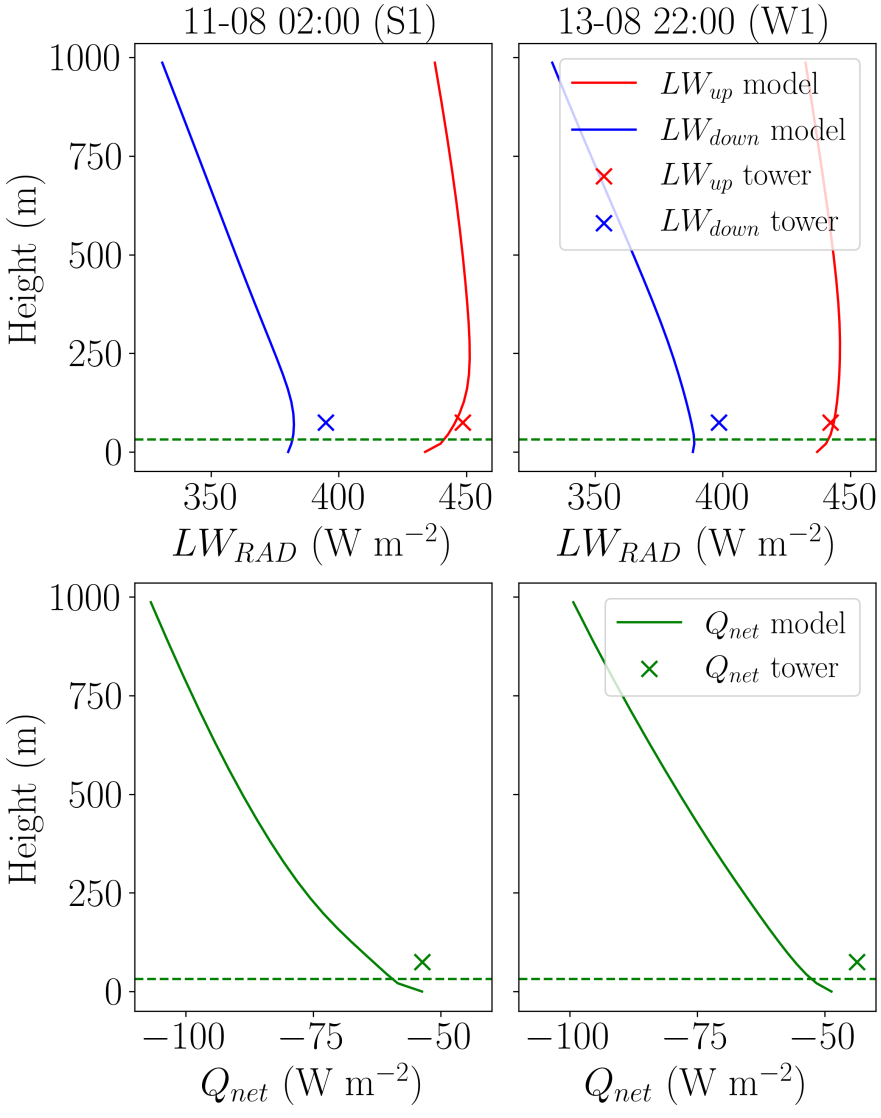


**Figure A2.** RTE+RRTMGP model output for S1 and W1. For the upgoing (red) and downward (blue) longwave radiation, and net longwave radiation (green). Together with the tower observations at 75 m (x).

*Acknowledgements.* The CloudRoots-Amazon22 campaign was funded by the Dutch Research Council (NWO under the project CloudRoots–Clouds rooted in a heterogeneous biosphere (https://cloudroots.wur.nl/) (Dutch Research Council NWO OCENW.KLEIN.407). Additionally, this study was supported by the Amazon Tall Tower Observatory (ATTO), funded by the German Federal Ministry of Education and Research (BMBF, contracts 01LB1001A, and 01LK1602A), the Brazilian Ministry of Science, Technology and Innovation (MCTI/FINEP, contract 01.11.01248.00) and the Max Planck Society (MPG). ATTO is also supported by the Fundação de Amparo à Pesquisa do Estado do Amazonas (FAPEAM), Fundação de Amparo à Pesquisa do Estado de São Paulo (FAPESP), Universidade do Estado do Amazonas

https://doi.org/10.5194/egusphere-2026-684
Preprint. Discussion started: 17 February 2026


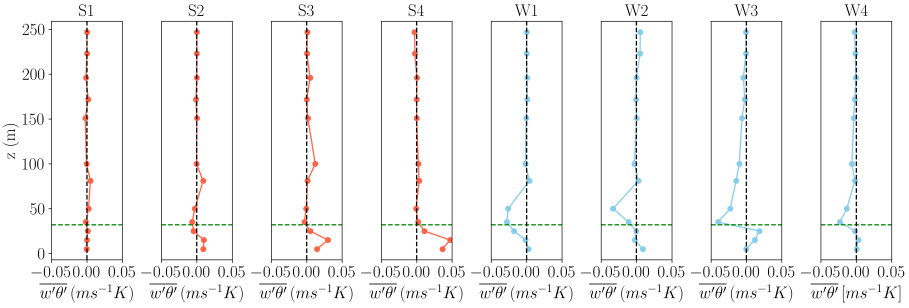


**Figure B1.** *Eddy covariance heat fluxes above and below the canopy for the selected strongly and weakly stable periods. The canopy top (32 m) is depicted by the horizontal green dashed line.*

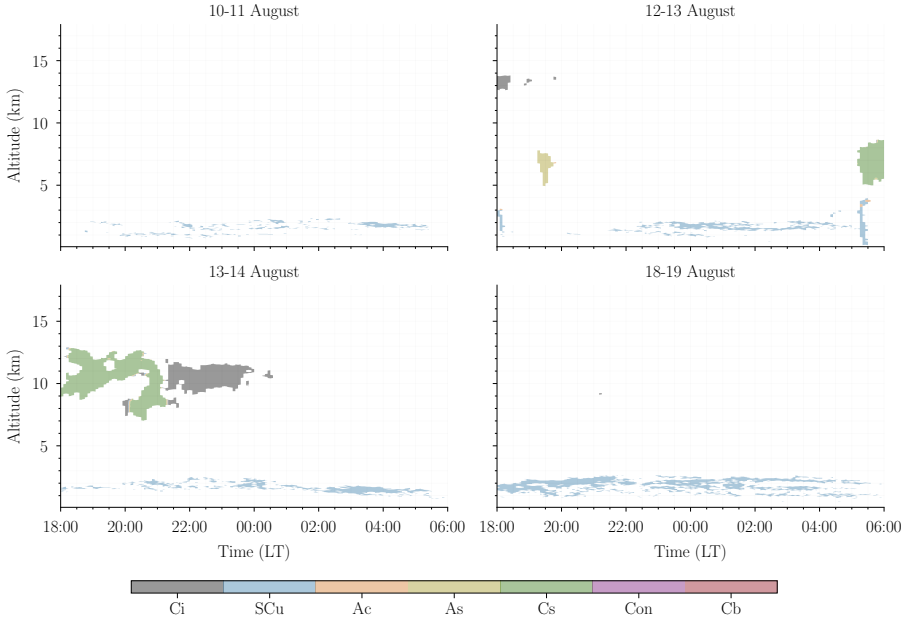


**Figure C1.** *Clouds observed by the MIRA Doppler radar, during the nights of 10-11 August, 12-13 August, 13-14 August and 18-19 August. Where the nights start at sunset at 18:00 and end at sunrise at 06:00. In the figure, the cloud abbreviations mean the following: cirrus (Ci), shallow cumulus (SCu), altocumulus (Ac), altostratus (As), cirrostratus (Cs), cumulus congestus (Con) and cumulonimbus (Cb).*

(UEA), Instituto Nacional de Pesquisas Amazônia (INPA), Programa de Grande Escala da Biosfera-Atmosfera na Amazônia (LBA) and the SDS/CEUC/RDS-Uatumã.

https://doi.org/10.5194/egusphere-2026-684
Preprint. Discussion started: 17 February 2026


## References

Acevedo, O. C., da Silva, R., Fitzjarrald, D. R., Moraes, O. L. L., Sakai, R. K., and Czikowsky, M. J.: Nocturnal vertical CO2 accumulation in two Amazonian ecosystems, Journal of Geophysical Research: Biogeosciences, 113, https://doi.org/https://doi.org/10.1029/2007JG000612, 2008.

Acevedo, O. C., Mahrt, L., Puhales, F. S., Costa, F. D., Medeiros, L. E., and Degrazia, G. A.: Contrasting structures between the decoupled and coupled states of the stable boundary layer, Quarterly Journal of the Royal Meteorological Society, 142, 693–702, https://doi.org/https://doi.org/10.1002/qj.2693, 2016.

Al-Kayssi, A. W., Al-Karaghouli, A. A., Hasson, A. M., and Beker, S. A.: Influence of soil moisture content on soil temperature and heat storage under greenhouse conditions, Journal of Agricultural Engineering Research, 45, 241–252, https://doi.org/https://doi.org/10.1016/S0021-8634(05)80152-0, 1990.

André, J. C., De Moor, G., Lacarrère, P., and du Vachat, R.: Modeling the 24-Hour Evolution of the Mean and Turbulent Structures of the Planetary Boundary Layer, Journal of Atmospheric Sciences, 35, 1861–1883, https://doi.org/https://doi.org/10.1175/1520-0469(1978)035<1861:MTHEOT>2.0.CO;2, 1978.

Andreae, M. O., Acevedo, O. C., Araùjo, A., Artaxo, P., Barbosa, C. G. G., Barbosa, H. M. J., Brito, J., Carbone, S., Chi, X., Cintra, B. B. L., da Silva, N. F., Dias, N. L., Dias-Júnior, C. Q., Ditas, F., Ditz, R., Godoi, A. F. L., Godoi, R. H. M., Heimann, M., Hoffmann, T., Kesselmeier, J., Könemann, T., Krüger, M. L., Lavric, J. V., Manzi, A. O., Lopes, A. P., Martins, D. L., Mikhailov, E. F., Moran-Zuloaga, D., Nelson, B. W., Nölscher, A. C., Santos Nogueira, D., Piedade, M. T. F., Pöhlker, C., Pöschl, U., Quesada, C. A., Rizzo, L. V., Ro, C.-U., Ruckteschler, N., Sá, L. D. A., de Oliveira Sá, M., Sales, C. B., dos Santos, R. M. N., Saturno, J., Schöngart, J., Sörgel, M., de Souza, C. M., de Souza, R. A. F., Su, H., Targhetta, N., Tóta, J., Trebs, I., Trumbore, S., van Eijck, A., Walter, D., Wang, Z., Weber, B., Williams, J., Winderlich, J., Wittmann, F., Wolff, S., and Yáñez-Serrano, A. M.: The Amazon Tall Tower Observatory (ATTO): overview of pilot measurements on ecosystem ecology, meteorology, trace gases, and aerosols, Atmospheric Chemistry and Physics, 15, 10 723–10 776, https://doi.org/10.5194/acp-15-10723-2015, 2015.

Anton Beljaars, Gianpaolo Balsamo, Alan Betts, Emanuel Dutra, Anna Ghelli, Martin Köhler, Irina Sandu, Soumia Serrar, and Pedro Viterbo: The stable boundary layer in the ECMWF model, Tech. rep., ECMWF, 2011.

Aragão, L. E. O. C., Poulter, B., Barlow, J. B., Anderson, L. O., Malhi, Y., Saatchi, S., Phillips, O. L., and Gloor, E.: Environmental change and the carbon balance of Amazonian forests, Biological Reviews, 89, 913–931, https://doi.org/https://doi.org/10.1111/brv.12088, 2014.

Aubinet, M.: Eddy covariance CO2 flux measurements in nocturnal conditions: an analysis of the problem, Ecological Applications, 18, 1368–1378, https://doi.org/https://doi.org/10.1890/06-1336.1, 2008.

Aubinet, M., Grelle, A., Ibrom, A., Rannik, , Moncrieff, J., Foken, T., Kowalski, A. S., Martin, P. H., Berbigier, P., Bernhofer, C., Clement, R., Elbers, J., Granier, A., Grünwald, T., Morgenstern, K., Pilegaard, K., Rebmann, C., Snijders, W., Valentini, R., and Vesala, T.: Estimates of the Annual Net Carbon and Water Exchange of Forests: The EUROFLUX Methodology, in: Advances in Ecological Research, edited by Fitter, A. H. and Raffaelli, D. G., vol. 30, pp. 113–175, Academic Press, ISBN 0065-2504, https://doi.org/https://doi.org/10.1016/S0065-2504(08)60018-5, 1999.

Banta, R. M., Pichugina, Y. L., and Newsom, R. K.: Relationship between Low-Level Jet Properties and Turbulence Kinetic Energy in the Nocturnal Stable Boundary Layer, Journal of the Atmospheric Sciences, 60, 2549 – 2555, https://doi.org/10.1175/1520-0469(2003)060<2549:RBLJPA>2.0.CO;2, 2003.

https://doi.org/10.5194/egusphere-2026-684
Preprint. Discussion started: 17 February 2026


Blackadar, A. K.: Boundary Layer Wind Maxima and Their Significance for the Growth of Nocturnal Inversions, Bulletin of the American Meteorological Society, 38, 283–290, https://doi.org/https://doi.org/10.1175/1520-0477-38.5.283, 1957.

Bonan, G. B., Patton, E. G., Harman, I. N., Oleson, K. W., Finnigan, J. J., Lu, Y., and Burakowski, E. A.: Modeling canopy-induced turbulence in the Earth system: a unified

585 }parameterization of turbulent exchange within plant canopies and the

}roughness sublayer (CLM-ml v0), Geoscientific Model Development, 11, 1467–1496, https://doi.org/10.5194/gmd-11-1467-2018, 2018.

Bonan, G. B., Patton, E. G., Finnigan, J. J., Baldocchi, D. D., and Harman, I. N.: Moving beyond the incorrect but useful paradigm: reevaluating big-leaf and multilayer plant canopies to model biosphere-atmosphere fluxes – a review, Agricultural and Forest Meteorology, 306, 108 435, https://doi.org/https://doi.org/10.1016/j.agrformet.2021.108435, 2021.

590 Brienen, R. J. W., Phillips, O. L., Feldpausch, T. R., Gloor, E., Baker, T. R., Lloyd, J., Lopez-Gonzalez, G., Monteagudo-Mendoza, A., Malhi, Y., Lewis, S. L., Vásquez Martinez, R., Alexiades, M., Álvarez Dávila, E., Alvarez-Loayza, P., Andrade, A., Aragão, L. E. O. C., Araujo-Murakami, A., Arets, E. J. M. M., Arroyo, L., Aymard C., G. A., Bánki, O. S., Baraloto, C., Barroso, J., Bonal, D., Boot, R. G. A., Camargo, J. L. C., Castilho, C. V., Chama, V., Chao, K. J., Chave, J., Comiskey, J. A., Cornejo Valverde, F., da Costa, L., de Oliveira, E. A., Di Fiore, A., Erwin, T. L., Fauset, S., Forsthofer, M., Galbraith, D. R., Grahame, E. S., Groot, N., Hérault, B., Higuchi, N.,

595 Honorio Coronado, E. N., Keeling, H., Killeen, T. J., Laurance, W. F., Laurance, S., Licona, J., Magnussen, W. E., Marimon, B. S., Marimon-Junior, B. H., Mendoza, C., Neill, D. A., Nogueira, E. M., Núñez, P., Pallqui Camacho, N. C., Parada, A., Pardo-Molina, G., Peacock, J., Peña-Claros, M., Pickavance, G. C., Pitman, N. C. A., Poorter, L., Prieto, A., Quesada, C. A., Ramírez, F., Ramírez-Angulo, H., Restrepo, Z., Roopsind, A., Rudas, A., Salomão, R. P., Schwarz, M., Silva, N., Silva-Espejo, J. E., Silveira, M., Stropp, J., Talbot, J., ter Steege, H., Teran-Aguilar, J., Terborgh, J., Thomas-Caesar, R., Toledo, M., Torello-Raventos, M., Umetsu, R. K., van der Heijden, G.

600 M. F., van der Hout, P., Guimarães Vieira, I. C., Vieira, S. A., Vilanova, E., Vos, V. A., and Zagt, R. J.: Long-term decline of the Amazon carbon sink, Nature, 519, 344–348, https://doi.org/10.1038/nature14283, 2015.

Carneiro, R. G. and Fisch, G.: Observational analysis of the daily cycle of the planetary boundary layer in

}the central Amazon during a non-El Niño year and El Niño year (GoAmazon

}project 2014/5), Atmospheric Chemistry and Physics, 20, 5547–5558, https://doi.org/10.5194/acp-20-5547-2020, 2020.

605 Chen, B. and Chamecki, M.: Turbulent Kinetic Energy Budgets over Gentle Topography Covered by Forests, Journal of the Atmospheric Sciences, 80, 91–109, https://doi.org/https://doi.org/10.1175/JAS-D-22-0027.1, 2023.

Costa, M. H. and Foley, J. A.: Combined Effects of Deforestation and Doubled Atmospheric CO2 Concentrations on the Climate of Amazonia, Journal of Climate, 13, 18–34, https://doi.org/https://doi.org/10.1175/1520-0442(2000)013<0018:CEODAD>2.0.CO;2, 2000.

Culf, A. D., Fisch, G., Malhi, Y., and Nobre, C. A.: The influence of the atmospheric boundary layer on carbon dioxide concentrations over a

610 tropical forest, Agricultural and Forest Meteorology, 85, 149–158, https://doi.org/https://doi.org/10.1016/S0168-1923(96)02412-4, 1997.

Culf, A. D., Fisch, G., Malhi, Y., Carvalho Costa, R., Nobre, A. D., de O. Marques Filho, A., Gash, J. H. C., and Grace, J.: Carbon dioxide measurements in the nocturnal boundary layer over Amazonian forest, Hydrology and Earth System Sciences, 3, 39–53, https://doi.org/10.5194/hess-3-39-1999, 1999.

Cuxart, J., Holtslag, A. A. M., Beare, R. J., Bazile, E., Beljaars, A., Cheng, A., Conangla, L., Ek, M., Freedman, F., Hamdi, R., Kerstein,

615 A., Kitagawa, H., Lenderink, G., Lewellen, D., Mailhot, J., Mauritsen, T., Perov, V., Schayes, G., Steeneveld, G.-J., Svensson, G., Taylor, P., Weng, W., Wunsch, S., and Xu, K.-M.: Single-Column Model Intercomparison for a Stably Stratified Atmospheric Boundary Layer, Boundary-Layer Meteorology, 118, 273–303, https://doi.org/10.1007/s10546-005-3780-1, 2006.

https://doi.org/10.5194/egusphere-2026-684
Preprint. Discussion started: 17 February 2026


de Abreu Sá, L. D., Viswanadham, Y., and Manzi, A. O.: Energy flux partitioning over the Amazon forest, Theoretical and Applied Climatology, 39, 1–16, https://doi.org/10.1007/BF00867653, 1988.

de Araújo, A. C., Dolman, A. J., Waterloo, M. J., Gash, J. H. C., Kruijt, B., Zanchi, F. B., de Lange, J. M. E., Stoevelaar, R., Manzi, A. O., Nobre, A. D., Lootens, R. N., and Backer, J.: The spatial variability of CO2 storage and the interpretation of eddy covariance fluxes in central Amazonia, Agricultural and Forest Meteorology, 150, 226–237, https://doi.org/https://doi.org/10.1016/j.agrformet.2009.11.005, 2010.

de Feiter, V. S., Janssens, M., de Haas, S. E. M., Hartogensis, O. K., Dias-Junior, C. Q., van Asperen, H., Martins, G., Miller, J. B., and Vilà-Guerau de Arellano, J.: Turbulent Exchange of CO2 in the Lower Tropical Troposphere Across Clear-to-Cloudy Conditions, Journal of Geophysical Research: Atmospheres, 130, e2025JD044 231, https://doi.org/https://doi.org/10.1029/2025JD044231, 2025.

De Kauwe, M. G., Medlyn, B. E., Knauer, J., and Williams, C. A.: Ideas and perspectives: how coupled is the vegetation to the boundary layer?, Biogeosciences, 14, 4435–4453, https://doi.org/10.5194/bg-14-4435-2017, 2017.

Dias-Júnior, C. Q., Sá, L. D. A., Marques Filho, E. P., Santana, R. A., Mauder, M., and Manzi, A. O.: Turbulence regimes in the stable boundary layer above and within the Amazon forest, Agricultural and Forest Meteorology, 233, 122–132, https://doi.org/https://doi.org/10.1016/j.agrformet.2016.11.001, 2017.

Dupont, S., Irvine, M. R., and Bidot, C.: Morning Transition of the Coupled Vegetation Canopy and Atmospheric Boundary Layer Turbulence according to the Wind Intensity, Journal of the Atmospheric Sciences, 81, 1225–1249, https://doi.org/https://doi.org/10.1175/JAS-D-23-0201.1, 2024.

Dwyer, M. J., Patton, E. G., and Shaw, R. H.: Turbulent kinetic energy budgets from a large-eddy simulation of airflow above and within a forest canopy, Boundary-Layer Meteorology, 84, 23–43, https://doi.org/10.1023/A:1000301303543, 1997.

Garstang, M. and Fitzjarrald, D. R.: Observations of surface to atmosphere interactions in the tropics, Oxford University Press, ISBN 9780195112702, 1999.

Gash, J. H. C. and Nobre, C. A.: Climatic Effects of Amazonian Deforestation: Some Results from ABRACOS, Bulletin of the American Meteorological Society, 78, 823–830, https://doi.org/https://doi.org/10.1175/1520-0477(1997)078<0823:CEOADS>2.0.CO;2, 1997.

Gatti, L. V., Basso, L. S., Miller, J. B., Gloor, M., Gatti Domingues, L., Cassol, H. L. G., Tejada, G., Aragão, L. E. O. C., Nobre, C., Peters, W., Marani, L., Arai, E., Sanches, A. H., Corrêa, S. M., Anderson, L., Von Randow, C., Correia, C. S. C., Crispim, S. P., and Neves, R. A. L.: Amazonia as a carbon source linked to deforestation and climate change, Nature, 595, 388–393, https://doi.org/10.1038/s41586-021-03629-6, 2021.

González-Armas, R., Rikkers, D., Hartogensis, O., Dias-Júnior, C. Q., Komiya, S., Pugliese, G., Williams, J., van Asperen, H., Vilà-Guerau de Arellano, J., and de Boer, H. J.: Daytime water and CO2 exchange within and above the Amazon rainforest, Agricultural and Forest Meteorology, 372, 110 621, https://doi.org/https://doi.org/10.1016/j.agrformet.2025.110621, 2025.

Goulden, M. L., Munger, J. W., Fan, S.-M., Daube, B. C., and Wofsy, S. C.: Measurements of carbon sequestration by long-term eddy covariance: methods and a critical evaluation of accuracy, Global Change Biology, 2, 169–182, https://doi.org/https://doi.org/10.1111/j.1365-2486.1996.tb00070.x, 1996.

Goulden, M. L., Miller, S. D., and da Rocha, H. R.: Nocturnal cold air drainage and pooling in a tropical forest, Journal of Geophysical Research: Atmospheres, 111, https://doi.org/https://doi.org/10.1029/2005JD006037, 2006.

Grachev, A. A., Andreas, E. L., Fairall, C. W., Guest, P. S., and Persson, P. O. G.: The Critical Richardson Number and Limits of Applicability of Local Similarity Theory in the Stable Boundary Layer, Boundary-Layer Meteorology, 147, 51–82, https://doi.org/10.1007/s10546-012-9771-0, 2013.

https://doi.org/10.5194/egusphere-2026-684
Preprint. Discussion started: 17 February 2026


Harris, N. L., Gibbs, D. A., Baccini, A., Birdsey, R. A., de Bruin, S., Farina, M., Fatoyinbo, L., Hansen, M. C., Herold, M., Houghton, R. A., Potapov, P. V., Suarez, D. R., Roman-Cuesta, R. M., Saatchi, S. S., Slay, C. M., Turubanova, S. A., and Tyukavina, A.: Global maps of twenty-first century forest carbon fluxes, Nature Climate Change, 11, 234–240, https://doi.org/10.1038/s41558-020-00976-6, 2021.

Hawkins, E. and Sutton, R.: The Potential to Narrow Uncertainty in Regional Climate Predictions, Bulletin of the American Meteorological Society, 90, 1095–1108, https://doi.org/https://doi.org/10.1175/2009BAMS2607.1, 2009.

Henkes, A., Fisch, G., Machado, L. A. T., and Chaboureau, J.-P.: Morning boundary layer conditions for shallow to deep convective cloud evolution during the dry season in the central Amazon, Atmospheric Chemistry and Physics, 21, 13 207–13 225, https://doi.org/10.5194/acp-21-13207-2021, 2021.

Hersbach, H., Bell, B., Berrisford, P., Hirahara, S., Horányi, A., Muñoz-Sabater, J., Nicolas, J., Peubey, C., Radu, R., Schepers, D., Simmons, A., Soci, C., Abdalla, S., Abellan, X., Balsamo, G., Bechtold, P., Biavati, G., Bidlot, J., Bonavita, M., De Chiara, G., Dahlgren, P., Dee, D., Diamantakis, M., Dragani, R., Flemming, J., Forbes, R., Fuentes, M., Geer, A., Haimberger, L., Healy, S., Hogan, R. J., Hólm, E., Janisková, M., Keeley, S., Laloyaux, P., Lopez, P., Lupu, C., Radnoti, G., de Rosnay, P., Rozum, I., Vamborg, F., Villaume, S., and Thépaut, J.-N.: The ERA5 global reanalysis, Quarterly Journal of the Royal Meteorological Society, 146, 1999–2049, https://doi.org/https://doi.org/10.1002/qj.3803, 2020.

Hubau, W., Lewis, S. L., Phillips, O. L., Affum-Baffoe, K., Beeckman, H., Cuní-Sanchez, A., Daniels, A. K., Ewango, C. E. N., Fauset, S., Mukinzi, J. M., Sheil, D., Sonké, B., Sullivan, M. J. P., Sunderland, T. C. H., Taedoumg, H., Thomas, S. C., White, L. J. T., Abernethy, K. A., Adu-Bredu, S., Amani, C. A., Baker, T. R., Banin, L. F., Baya, F., Begne, S. K., Bennett, A. C., Benedet, F., Bitariho, R., Bocko, Y. E., Boeckx, P., Boundja, P., Brienen, R. J. W., Brncic, T., Chezeaux, E., Chuyong, G. B., Clark, C. J., Collins, M., Comiskey, J. A., Coomes, D. A., Dargie, G. C., de Haulleville, T., Kamdem, M. N. D., Doucet, J.-L., Esquivel-Muelbert, A., Feldpausch, T. R., Fofanah, A., Foli, E. G., Gilpin, M., Gloor, E., Gonmadje, C., Gourlet-Fleury, S., Hall, J. S., Hamilton, A. C., Harris, D. J., Hart, T. B., Hockemba, M. B. N., Hladik, A., Ifo, S. A., Jeffery, K. J., Jucker, T., Yakusu, E. K., Kearsley, E., Kenfack, D., Koch, A., Leal, M. E., Levesley, A., Lindsell, J. A., Lisingo, J., Lopez-Gonzalez, G., Lovett, J. C., Makana, J.-R., Malhi, Y., Marshall, A. R., Martin, J., Martin, E. H., Mbayu, F. M., Medjibe, V. P., Mihindou, V., Mitchard, E. T. A., Moore, S., Munishi, P. K. T., Bengone, N. N., Ojo, L., Ondo, F. E., Peh, K. S.-H., Pickavance, G. C., Poulsen, A. D., Poulsen, J. R., Qie, L., Reitsma, J., Rovero, F., Swaine, M. D., Talbot, J., Taplin, J., Taylor, D. M., Thomas, D. W., Toirambe, B., Mukendi, J. T., Tuagben, D., Umunay, P. M., van der Heijden, G. M. F., Verbeeck, H., Vleminckx, J., Willcock, S., Wöll, H., Woods, J. T., and Zemagho, L.: Asynchronous carbon sink saturation in African and Amazonian tropical forests, Nature, 579, 80–87, https://doi.org/10.1038/s41586-020-2035-0, 2020.

IPCC: IPCC 2023: Climate Change 2023: Synthesis Report. Contribution of Working Groups I, II and III to the Sixth Assessment Report of the Intergovernmental Panel on Climate Change, Tech. rep., IPCC, Geneva, 2023.

Karipot, A., Leclerc, M. Y., Zhang, G., Martin, T., Starr, G., Hollinger, D., McCaughey, J. H., and Hendrey, G. R.: Nocturnal CO2 exchange over a tall forest canopy associated with intermittent low-level jet activity, Theoretical and Applied Climatology, 85, 243–248, https://doi.org/10.1007/s00704-005-0183-7, 2006.

Khanna, J. and Medvigy, D.: Strong control of surface roughness variations on the simulated dry season regional atmospheric response to contemporary deforestation in Rondônia, Brazil, Journal of Geophysical Research: Atmospheres, 119, 13–67, https://doi.org/https://doi.org/10.1002/2014JD022278, 2014.

Lloyd, J. and Taylor, J. A.: On the Temperature Dependence of Soil Respiration, Functional Ecology, 8, 315–323, https://doi.org/10.2307/2389824, 1994.

https://doi.org/10.5194/egusphere-2026-684
Preprint. Discussion started: 17 February 2026


Lloyd, J., Kolle, O., Fritsch, H., de Freitas, S. R., Silva Dias, M. A. F., Artaxo, P., Nobre, A. D., de Araújo, A. C., Kruijt, B., Sogacheva, L., Fisch, G., Thielmann, A., Kuhn, U., and Andreae, M. O.: An airborne regional carbon balance for Central Amazonia, Biogeosciences, 4, 759–768, https://doi.org/10.5194/bg-4-759-2007, 2007.

Loescher, H. W., Law, B. E., Mahrt, L., Hollinger, D. Y., Campbell, J., and Wofsy, S. C.: Uncertainties in, and interpretation of, carbon flux estimates using the eddy covariance technique, Journal of Geophysical Research: Atmospheres, 111, https://doi.org/https://doi.org/10.1029/2005JD006932, 2006.

Ma, Y. and Liu, H.: An Advanced Multiple-Layer Canopy Model in the WRF Model With Large-Eddy Simulations to Simulate Canopy Flows and Scalar Transport Under Different Stability Conditions, Journal of Advances in Modeling Earth Systems, 11, 2330–2351, https://doi.org/https://doi.org/10.1029/2018MS001347, 2019.

Machado, L. A. T., Kesselmeier, J., Bot\'{\i}a, S., van Asperen, H., O. Andreae, M., de Araújo, A. C., Artaxo, P., Edtbauer, A., R. Ferreira, R., Franco, M. A., Harder, H., Jones, S. P., Dias-Júnior, C. Q., Haytzmann, G. G., Quesada, C. A., Komiya, S., Lavric, J., Lelieveld, J., Levin, I., Nölscher, A., Pfannerstill, E., Pöhlker, M. L., Pöschl, U., Ringsdorf, A., Rizzo, L., Yáñez-Serrano, A. M., Trumbore, S., Valenti, W. I. D., de Arellano, J., Walter, D., Williams, J., Wolff, S., and Pöhlker, C.: How rainfall events modify trace gas mixing ratios in central Amazonia, Atmospheric Chemistry and Physics, 24, 8893–8910, https://doi.org/10.5194/acp-24-8893-2024, 2024.

Mahrt, L.: Nocturnal Boundary-Layer Regimes, Boundary-Layer Meteorology, 88, 255–278, https://doi.org/10.1023/A:1001171313493, 1998.

Mahrt, L.: Stratified Atmospheric Boundary Layers, Boundary-Layer Meteorology, 90, 375–396, https://doi.org/10.1023/A:1001765727956, 1999.

Mahrt, L.: The Near-Calm Stable Boundary Layer, Boundary-Layer Meteorology, 140, 343–360, https://doi.org/10.1007/s10546-011-9616-2, 2011.

Mahrt, L., Heald, R. C., Lenschow, D. H., Stankov, B. B., and Troen, I. B.: An observational study of the structure of the nocturnal boundary layer, Boundary-Layer Meteorology, 17, 247–264, https://doi.org/10.1007/BF00117983, 1979.

Mendonça, A. C. S., Dias-Júnior, C. Q., Acevedo, O. C., Santana, R. A., Costa, F. D., Negrón-Juarez, R. I., Manzi, A. O., Trumbore, S. E., and Marra, D. M.: Turbulence regimes in the nocturnal roughness sublayer: Interaction with deep convection and tree mortality in the Amazon, Agricultural and Forest Meteorology, 339, 109 526, https://doi.org/https://doi.org/10.1016/j.agrformet.2023.109526, 2023.

Mendonça, A. C. S., Dias-Júnior, C. Q., Acevedo, O. C., Marra, D. M., Cely-Toro, I. M., Fisch, G., Brondani, D. V., Manzi, A. O., Portela, B. T. T., Quesada, C. A., and Mortarini, L.: Estimation of the nocturnal boundary layer height over the Central Amazon forest using turbulence measurements, Agricultural and Forest Meteorology, 367, 110 469, https://doi.org/https://doi.org/10.1016/j.agrformet.2025.110469, 2025a.

Mendonça, A. C. S., Dias-Júnior, C. Q., Martins, L. G. N., Marra, D. M., Costa, F. D., Maroneze, R., Fisch, G., de Oliveira, R. S., Portela, B. T. T., and Acevedo, O. C.: Can wind profiles accurately estimate nocturnal boundary layer height during low-level jets? (under review), Agricultural and Forest Meteorology, 2025b.

Mironov, D. V. and Sullivan, P. P.: Second-Moment Budgets and Mixing Intensity in the Stably Stratified Atmospheric Boundary Layer over Thermally Heterogeneous Surfaces, Journal of the Atmospheric Sciences, 73, 449 – 464, https://doi.org/10.1175/JAS-D-15-0075.1, 2016.

Moonen, R. P. J., Adnew, G. A., de Arellano, J., Hartogensis, O. K., Bonell Fontas, D. J., Komiya, S., Jones, S. P., and Röckmann, T.: Amazon rainforest ecosystem exchange of CO_2 and H_2O through turbulent understory ejections, Atmospheric Chemistry and Physics, 25, 12 197–12 212, https://doi.org/10.5194/acp-25-12197-2025, 2025.

https://doi.org/10.5194/egusphere-2026-684
Preprint. Discussion started: 17 February 2026


Oliveira, P. E. S., Acevedo, O. C., Moraes, O. L. L., Zimermann, H. R., and Teichrieb, C.: Nocturnal Intermittent Coupling Between the Interior of a Pine Forest and the Air Above It, Boundary-Layer Meteorology, 146, 45–64, https://doi.org/10.1007/s10546-012-9756-z, 2013.

Oliveira, P. E. S., Acevedo, O. C., Sörgel, M., Tsokankunku, A., Wolff, S., Araújo, A. C., Souza, R. A. F., Sá, M. O., Manzi, A. O., and Andreae, M. O.: Nighttime wind and scalar variability within and above an Amazonian canopy, Atmospheric Chemistry and Physics, 18, 3083–3099, https://doi.org/10.5194/acp-18-3083-2018, 2018.

Pedruzo-Bagazgoitia, X., Patton, E. G., Moene, A. F., Ouwersloot, H. G., Gerken, T., Machado, L. A. T., Martin, S. T., Sörgel, M., Stoy, P. C., Yamasoe, M. A., and Vilà-Guerau de Arellano, J.: Investigating the Diurnal Radiative, Turbulent, and Biophysical Processes in the Amazonian Canopy-Atmosphere Interface by Combining LES Simulations and Observations, Journal of Advances in Modeling Earth Systems, 15, e2022MS003 210, https://doi.org/https://doi.org/10.1029/2022MS003210, 2023.

Pincus, R., Mlawer, E. J., and Delamere, J. S.: Balancing Accuracy, Efficiency, and Flexibility in Radiation Calculations for Dynamical Models, Journal of Advances in Modeling Earth Systems, 11, 3074–3089, https://doi.org/https://doi.org/10.1029/2019MS001621, 2019.

Rosan, T. M., Sitch, S., O'Sullivan, M., Basso, L. S., Wilson, C., Silva, C., Gloor, E., Fawcett, D., Heinrich, V., Souza, J. G., Bezerra, F. G. S., von Randow, C., Mercado, L. M., Gatti, L., Wiltshire, A., Friedlingstein, P., Pongratz, J., Schwingshackl, C., Williams, M., Smallman, L., Knauer, J., Arora, V., Kennedy, D., Tian, H., Yuan, W., Jain, A. K., Falk, S., Poulter, B., Arneth, A., Sun, Q., Zaehle, S., Walker, A. P., Kato, E., Yue, X., Bastos, A., Ciais, P., Wigneron, J.-P., Albergel, C., and Aragão, L. E. O. C.: Synthesis of the land carbon fluxes of the Amazon region between 2010 and 2020, Communications Earth & Environment, 5, 46, https://doi.org/10.1038/s43247-024-01205-0, 2024.

Santos, D. M., Acevedo, O. C., Chamecki, M., Fuentes, J. D., Gerken, T., and Stoy, P. C.: Temporal Scales of the Nocturnal Flow Within and Above a Forest Canopy in Amazonia, Boundary-Layer Meteorology, 161, 73–98, https://doi.org/10.1007/s10546-016-0158-5, 2016.

Science Panel for the Amazon.: Amazon Assessment Report 2021 , Tech. rep., https://www.theamazonwewant.org/spa_publication/amazon-assessment-report-2021/, 2021.

Smedman, A.-S.: Observations of a multi-level turbulence structure in a very stable atmospheric boundary layer, Boundary-Layer Meteorology, 44, 231–253, https://doi.org/10.1007/BF00116064, 1988.

Stull: An Introduction to Boundary Layer Meteorology, Kluwer Academic, Dordrecht, 1988.

Sun, J., Mahrt, L., Banta, R. M., and Pichugina, Y. L.: Turbulence Regimes and Turbulence Intermittency in the Stable Boundary Layer during CASES-99, Journal of the Atmospheric Sciences, 69, 338 – 351, https://doi.org/10.1175/JAS-D-11-082.1, 2012.

Svensson, G., Holtslag, A. A. M., Kumar, V., Mauritsen, T., Steeneveld, G. J., Angevine, W. M., Bazile, E., Beljaars, A., de Bruijn, E. I. F., Cheng, A., Conangla, L., Cuxart, J., Ek, M., Falk, M. J., Freedman, F., Kitagawa, H., Larson, V. E., Lock, A., Mailhot, J., Masson, V., Park, S., Pleim, J., Söderberg, S., Weng, W., and Zampieri, M.: Evaluation of the Diurnal Cycle in the Atmospheric Boundary Layer Over Land as Represented by a Variety of Single-Column Models: The Second GABLS Experiment, Boundary-Layer Meteorology, 140, 177–206, https://doi.org/10.1007/s10546-011-9611-7, 2011.

Van de Wiel, B. J. H., Moene, A. F., Ronda, R. J., De Bruin, H. A. R., and Holtslag, A. A. M.: Intermittent Turbulence and Oscillations in the Stable Boundary Layer over Land. Part II: A System Dynamics Approach, Journal of the Atmospheric Sciences, 59, 2567–2581, https://doi.org/https://doi.org/10.1175/1520-0469(2002)059<2567:ITAOIT>2.0.CO;2, 2002a.

Van de Wiel, B. J. H., Ronda, R. J., Moene, A. F., De Bruin, H. A. R., and Holtslag, A. A. M.: Intermittent Turbulence and Oscillations in the Stable Boundary Layer over Land. Part I: A Bulk Model, Journal of the Atmospheric Sciences, 59, 942–958, https://doi.org/https://doi.org/10.1175/1520-0469(2002)059<0942:ITAOIT>2.0.CO;2, 2002b.

https://doi.org/10.5194/egusphere-2026-684
Preprint. Discussion started: 17 February 2026


van Heerwaarden, C., Alessio Sclocco, I., Veerman, M., Powell, M., van Stratum, B., van Werkhoven, B., van den Oord, G., Pincus, R., and Tijhuis, M.: microhh / rte-rrtmgp-cpp, 2025.

van Stratum, B. J. H. and Stevens, B.: The influence of misrepresenting the nocturnal boundary layer on idealized daytime convection in large-eddy simulation, Journal of Advances in Modeling Earth Systems, 7, 423–436, https://doi.org/https://doi.org/10.1002/2014MS000370, 2015.

van Stratum, B. J. H., van Heerwaarden, C. C., and Vilà-Guerau de Arellano, J.: The Benefits and Challenges of Downscaling a Global Reanalysis With Doubly-Periodic Large-Eddy Simulations, Journal of Advances in Modeling Earth Systems, 15, e2023MS003 750, https://doi.org/https://doi.org/10.1029/2023MS003750, 2023.

Vickers, D. and Thomas, C. K.: Some aspects of the turbulence kinetic energy and fluxes above and beneath a tall open pine forest canopy, Agricultural and Forest Meteorology, 181, 143–151, https://doi.org/https://doi.org/10.1016/j.agrformet.2013.07.014, 2013.

Vilà-Guerau de Arellano, J., Hartogensis, O., Benedict, I., de Boer, H., Bosman, P. J. M., Botía, S., Cecchini, M. A., Faassen, K. A. P., González-Armas, R., van Diepen, K., Heusinkveld, B. G., Janssens, M., Lobos-Roco, F., Luijkx, I. T., Machado, L. A. T., Mangan, M. R., Moene, A. F., Mol, W. B., van der Molen, M., Moonen, R., Ouwersloot, H. G., Park, S.-W., Pedruzo-Bagazgoitia, X., Röckmann, T., Adnew, G. A., Ronda, R., Sikma, M., Schulte, R., van Stratum, B. J. H., Veerman, M. A., van Zanten, M. C., and van Heerwaarden, C. C.: Advancing understanding of land–atmosphere interactions by breaking discipline and scale barriers, Annals of the New York Academy of Sciences, 1522, 74–97, https://doi.org/https://doi.org/10.1111/nyas.14956, 2023.

Vilà-Guerau de Arellano, J., Hartogensis, O. K., de Boer, H., Moonen, R., González-Armas, R., Janssens, M., Adnew, G. A., Bonell-Fontás, D. J., Botía, S., Jones, S. P., van Asperen, H., Komiya, S., de Feiter, V. S., Rikkers, D., de Haas, S., Machado, L. A. T., Dias-Junior, C. Q., Giovanelli-Haytzmann, G., Valenti, W. I. D., Figueiredo, R. C., Farias, C. S., Hall, D. H., Mendonça, A. C. S., da Silva, F. A. G., Marton da Silva, J. L., Souza, R., Martins, G., Miller, J. N., Mol, W. B., Heusinkveld, B., van Heerwaarden, C. C., D'Oliveira, F. A. F., Rodrigues Ferreira, R., Gotuzzo, R. A., Pugliese, G., Williams, J., Ringsdorf, A., Edtbauer, A., Quesada, C. A., Takeshi Tanaka Portela, B., Gomes Alves, E., Pöhlker, C., Trumbore, S., Lelieveld, J., and Röckmann, T.: CloudRoots-Amazon22: Integrating Clouds with Photosynthesis by Crossing Scales, Bulletin of the American Meteorological Society, 105, E1275–E1302, https://doi.org/https://doi.org/10.1175/BAMS-D-23-0333.1, 2024.